A THREE-DIMENSIONAL NUMERICAL SENSITIVITY STUDY OF CONVECTION OVER THE FLORIDA PENINSULA

ZAFER BOYBEYI and SETHU RAMAN

Department of Marine, Earth and Atmospheric Sciences, North Carolina State University, Raleigh, NC 27695-8208, U.S.A.

(Received in final form 28 January, 1992)

Abstract. The Florida peninsula has the highest annual number of days with thunderstorms in the United States, partly due to sea breeze convergence. A three-dimensional mesoscale planetary boundary layer (PBL) model with the E-ϵ turbulence closure is used to investigate the relationship between sea breeze convergence and convection over the peninsula for two ambient wind cases during typical summer days.

It is found that the spatial and temporal variation of the sea breeze convergence zones and the associated convective activities depend to a large extent on the direction and magnitude of the ambient wind. For the case of southeasterly ambient winds, a strong convergence zone and hence significant rainfall occur primarily along the west coast of the peninsula. The convergence zone and the associated rainfall shift towards the east coast for the case of southwesterly ambient winds. These are in agreement with the observations. In contrast to the southeasterly and southwesterly ambient winds, an intense convergence zone and rainfall occur near both coastlines of the peninsula under light ambient winds.

It is also found that lake Okeechobee has a substantial influence on south Florida's mesoscale weather. A cloudless region is always present over the lake at least until late afternoon due to its own lake breeze circulation. Finally, increased roughness of the land surface appears to influence the temporal and spatial variation of the convection by determining the intensity of the vertical turbulent transport of heat and momentum.

1. Introduction

Mesoscale circulations associated with sea breezes have been investigated by both observational and modeling studies in the past (Fisher, 1961; Estoque, 1962; Neumann and Mahrer, 1971; Cotton *et al.*, 1976; Mahrer and Pielke, 1977). These studies have emphasized the effect of sea breeze convergence patterns on convection. A better understanding of the dynamics of the sea breeze and its relation to deep convection is thus important to improve mesoscale weather forecasting in coastal areas.

Due to its unique peninsular geography, Florida provides an excellent opportunity to investigate the relationship between sea breeze convergence and convective activities. The peninsula has the highest annual number of days with thunderstorms in the United States during summer days because of sea breeze convergence caused by differential heating between the peninsula and the ocean. The prevailing large-scale flow is generally from the southeast or the southwest depending on synoptic weather. Light winds are also often observed over the peninsula. These three significant wind patterns provide case studies for numerical simulations.

There have been several observational and modeling studies concerning the sea

Boundary-Layer Meteorology **60**: 325–359, 1992.

breeze over south Florida (Byers and Rodebush, 1948; Frank *et al.*, 1967; Pielke, 1974; Pielke and Cotton, 1977; Pielke and Mahrer; 1978) and central Florida (Neumann, 1971; Foote, 1991). Generally, these studies have concluded that mesoscale processes play an important role in determining the intensity and organization of cumulus convection in conjunction with the sea breezes on summer days. For example, Pielke (1974) examined the influence of two different wind directions on the development and movement of the predicted sea breeze convergence zones over south Florida by using a three-dimensional numerical mesoscale model. He concluded that dry sea breeze circulations have significant influence on the locations of thunderstorm complexes over south Florida on undisturbed summer days. The latter research (Cotton *et al.*, 1976) involved linkage of the mesoscale model developed by Pielke (1974) with the one-dimensional time-dependent cumulus cloud model developed by Cotton (1975) to examine the influence of the mesoscale circulation on the cumulus scale over south Florida. In this experiment, the one-dimensional cloud model was initiated with the theoretical soundings predicted by the mesoscale model.

The purpose of this study is to focus on the question of where and when a sea breeze convergence zone will develop and to determine whether it has the potential to produce strong convection and rainfall over the Florida peninsula for different ambient flows. It was felt that in order to address these questions, a mesoscale model capable of forecasting parameters related to convective activities is needed. Therefore, a numerical sensitivity study using a higher order turbulence closure three-dimensional mesoscale cloud model was conducted. The model used in this study has the required detailed moisture information to examine the complex interaction between the clouds and mesoscale air motions. It includes prognostic equations for water vapor, cloud water and rain water as well as boundary-layer and cumulus parameterizations. Also this work differs from previous studies in that the numerical study is conducted over the entire Florida peninsula. The numerical experiments are therefore designed to provide further insight into the complex interactions between deep precipitating cumulus clouds and mesoscale circulations over the entire Florida peninsula by examining the influence of the various synoptic environments on sea breezes.

2. Model Description

The mesoscale numerical model used in this study is identical to that used by Huang and Raman (1991a,b). Since a description of the model has been given by Huang (1990), only the forms of the equations are presented here. The model is hydrostatic and anelastic in a terrain-following coordinate system. The governing equations are given by

$$\frac{\partial u}{\partial t} = -u\frac{\partial u}{\partial x} - v\frac{\partial u}{\partial y} - \tilde{w}\frac{\partial u}{\partial \sigma} + fv - \theta_v\frac{\partial \pi}{\partial x} - g(1-\sigma)\frac{\partial \hat{E}}{\partial x}$$

$$+\frac{\partial}{\partial x}\left(K_H\frac{\partial u}{\partial x}\right)+\frac{\partial}{\partial y}\left(K_H\frac{\partial u}{\partial y}\right)+\frac{1}{H-\hat{E}}\frac{\partial}{\partial\sigma}(\overline{-u'w'}), \tag{1}$$

$$\frac{\partial v}{\partial t}=-u\frac{\partial v}{\partial x}-v\frac{\partial v}{\partial y}-\tilde{w}\frac{\partial v}{\partial\sigma}-fu-\theta_v\frac{\partial\pi}{\partial y}-g(1-\sigma)\frac{\partial\hat{E}}{\partial y}$$

$$+\frac{\partial}{\partial x}\left(K_H\frac{\partial v}{\partial x}\right)+\frac{\partial}{\partial y}\left(K_H\frac{\partial v}{\partial y}\right)+\frac{1}{H-\hat{E}}\frac{\partial}{\partial\sigma}(\overline{-v'w'}), \tag{2}$$

$$\frac{\partial\theta}{\partial t}=-u\frac{\partial\theta}{\partial x}-v\frac{\partial\theta}{\partial y}-\tilde{w}\frac{\partial\theta}{\partial\sigma}+\frac{\partial}{\partial x}\left(K_H\frac{\partial\theta}{\partial x}\right)+\frac{\partial}{\partial y}\left(K_H\frac{\partial\theta}{\partial y}\right)$$

$$+\frac{1}{H-\hat{E}}\frac{\partial}{\partial\sigma}(\overline{-w'\theta'})-\frac{L_c}{\pi}\left(\delta\frac{\mathrm{d}q_s}{\mathrm{d}t}\right)+Q_{\mathrm{CL}}-Q_{\mathrm{EV}}+Q_{\mathrm{RAD}}, \tag{3}$$

$$\frac{\partial q}{\partial t}=-u\frac{\partial q}{\partial x}-v\frac{\partial q}{\partial y}-\tilde{w}\frac{\partial q}{\partial\sigma}+\frac{\partial}{\partial x}\left(K_H\frac{\partial q}{\partial x}\right)+\frac{\partial}{\partial y}\left(K_H\frac{\partial q}{\partial y}\right)$$

$$+\frac{1}{H-\hat{E}}\frac{\partial}{\partial\sigma}(\overline{-w'q'})+\delta\frac{\mathrm{d}q_s}{\mathrm{d}t}+M_{\mathrm{CL}}+M_{\mathrm{EV}}, \tag{4}$$

$$\frac{\partial q_c}{\partial t}=-u\frac{\partial q_c}{\partial x}-v\frac{\partial q_c}{\partial y}-\tilde{w}\frac{\partial q_c}{\partial\sigma}+\frac{\partial}{\partial x}\left(K_H\frac{\partial q_c}{\partial x}\right)+\frac{\partial}{\partial y}\left(K_H\frac{\partial q_c}{\partial y}\right)$$

$$+\frac{1}{H-\hat{E}}\frac{\partial}{\partial\sigma}(\overline{-w'q_c'})-\delta\frac{\mathrm{d}q_s}{\mathrm{d}t}-M_{\mathrm{AC}}-M_{\mathrm{RV}}, \tag{5}$$

$$\frac{\partial q_r}{\partial t}=-u\frac{\partial q_r}{\partial x}-v\frac{\partial q_r}{\partial y}-\tilde{w}\frac{\partial q_r}{\partial\sigma}+\frac{\partial}{\partial x}\left(K_H\frac{\partial q_r}{\partial x}\right)+\frac{\partial}{\partial y}\left(K_H\frac{\partial q_r}{\partial y}\right)$$

$$+\frac{1}{H-\hat{E}}\frac{\partial}{\partial\sigma}(-\overline{w'q_r'})+M_{\mathrm{VT}}+M_{\mathrm{AC}}+M_{\mathrm{RV}}-M_{\mathrm{EV}}, \tag{6}$$

$$\frac{\partial\rho u(H-\hat{E})}{\partial x}+\frac{\partial\rho v(H-\hat{E})}{\partial y}+\frac{\partial\rho\tilde{w}(H-\hat{E})}{\partial\sigma}=0, \tag{7}$$

$$\frac{\partial\pi}{\partial\sigma}=-\frac{g(H-\hat{E})}{\theta_v}, \tag{8}$$

where the terrain-following coordinate is defined by

$$\sigma=\frac{z-\hat{E}}{H-\hat{E}},$$

with the model maximum height H and the terrain height $\hat{E}$. Equations (1) and (2) are the horizontal momentum equations for the east-west and north-south

wind components (u and v), respectively. Equation (3) is the thermodynamic equation for the potential temperature (θ). Equations (4), (5) and (6) are the conservation equations for water vapor (q), cloud water (q_c) and rain water (q_r), respectively. Equation (7) is the anelastic equation for fluid continuity. Equation (8) is the hydrostatic equation. In the prognostic equations (1) to (6), terms involving K_H are for horizontal diffusion and terms with primed variables are for subgrid turbulence flux divergence.

The PBL is treated in two parts as the surface layer and the transition layer. The similarity stability functions given by Businger *et al.* (1971) are used to account for surface-layer turbulent transport. Above the surface layer, a turbulence closure scheme using the turbulent kinetic energy (TKE) and dissipation (ϵ) is incorporated with the level 2.5 scheme of Mellor and Yamada (1982) to determine the eddy diffusivities in the transition layer.

To account for advection effects, a modified Warming–Kutler–Lomax (WKL) advection scheme (Warming *et al.*, 1973; Huang and Raman, 1990) is used in the horizontal and a quadratic upstream interpolation in the vertical. In order to obtain initial conditions, an Ekman-layer type balance equation is used to determine an initial velocity profile, while the potential temperature and relative humidity profiles are specified at the initial time. At the lower boundary, a no-slip condition is imposed for the wind. The sea surface temperature is fixed and the ground temperature is computed using the surface energy budget equation in which the longwave and shortwave radiation, the soil heat flux and the turbulent mixing of sensible and latent heat fluxes are used to calculate equilibrium surface temperatures. The relative humidity on the ground is held constant. The hydrostatic equation is used to obtain the surface pressure with the known upper level pressure. At the upper boundary, a radiation boundary condition (Klemp and Durran, 1983) is used to determine the upper perturbation pressure. For the prognostic variables, Orlanski's radiation condition (Orlanski, 1976) with forward-upstream scheme (Miller and Thorpe, 1981) is applied to the lateral inflow boundary grids, while the prediction equations are used at the lateral outflow boundary grids.

3. Numerical Experiments

The primary objective is to examine the influence of ambient wind direction and magnitude on the sea breeze patterns and associated convective activities. Six numerical sensitivity studies were conducted for a typical summer day with the assumption that neither tropical nor frontal systems were present for the period of simulation. Variations in topography were ignored as the peninsula is essentially flat.

Numerical experiments on Cases C1 and C2 are conducted to examine the influence of southeasterly and southwesterly ambient wind directions, respectively. The wind speed was assumed constant, its magnitude being a climatological average. Both wind directions are frequently observed over the Florida peninsula

TABLE I

Description of the numerical experiments

Cases	Geostrophic wind ($m\,s^{-1}$)		Direction	Notes
C1. The influence of a southeasterly wind	$Ug = -2.5$	$Vg = 2.5$	135°	
C2. The influence of a southwesterly wind	$Ug = 2.5$	$Vg = 2.5$	225°	
C3. The influence of lake Okeechobee for a southeasterly wind	$Ug = -2.5$	$Vg = 2.5$	135°	The lake is removed
C4. The influence of lake Okeechobee for a southwesterly wind	$Ug = 2.5$	$Vg = 2.5$	225°	The lake is removed
C5. The influence of surface roughness	$Ug = 2.5$	$Vg = 2.5$	225°	Charnock's relationship is used over both land and water
C6. The influence of light wind	$Ug = 0.1$	$Vg = 0.1$	225°	

during summer days. Since lake Okeechobee is one of the prominent geographical features in the Florida peninsula, it was felt that a study of the influence of the lake on south Florida's mesoscale weather would be of interest. Therefore, the influence of lake Okeechobee is examined for the two dominant ambient wind directions in Cases C3 and C4 by removing the lake from the model domain. Case C3 is for a southeasterly ambient wind direction, while Case C4 is for a southwesterly ambient wind direction without the lake. The differential heating and the surface roughness change between land and water are two important factors in causing mesoscale convergence. The relative importance of differential surface roughness on the mesoscale circulation is examined in Case C5 for a southwesterly ambient wind direction. Finally, Case C6 assumes light winds. A full description of all the cases is given in Table I.

Values of the other prescribed parameters and large-scale variables used in the model for all cases are identical and are given below. The model domain contains 22 grids in the vertical with the model top at 8 km. The horizontal domain includes 60 grids east-west and 70 grids north-south with a uniform grid interval of 10 km. Outline of the Florida peninsula and lake Okeechobee used in the model are shown in Figure 1 along with the non-staggered grid mesh. The model is integrated for 14 h to include the sea breeze heating cycle with an integration time interval of 30 s. The initial surface temperatures over both land and water are set at 25 °C consistent with the climatological observations; the variation of soil temperatures is then determined using diurnal heating. Relative humidity is assumed 80% below 2 km and then decreases linearly to zero at 5 km height. The surface roughness length is assumed to be 4 cm over land, while Charnock's relationship is used over

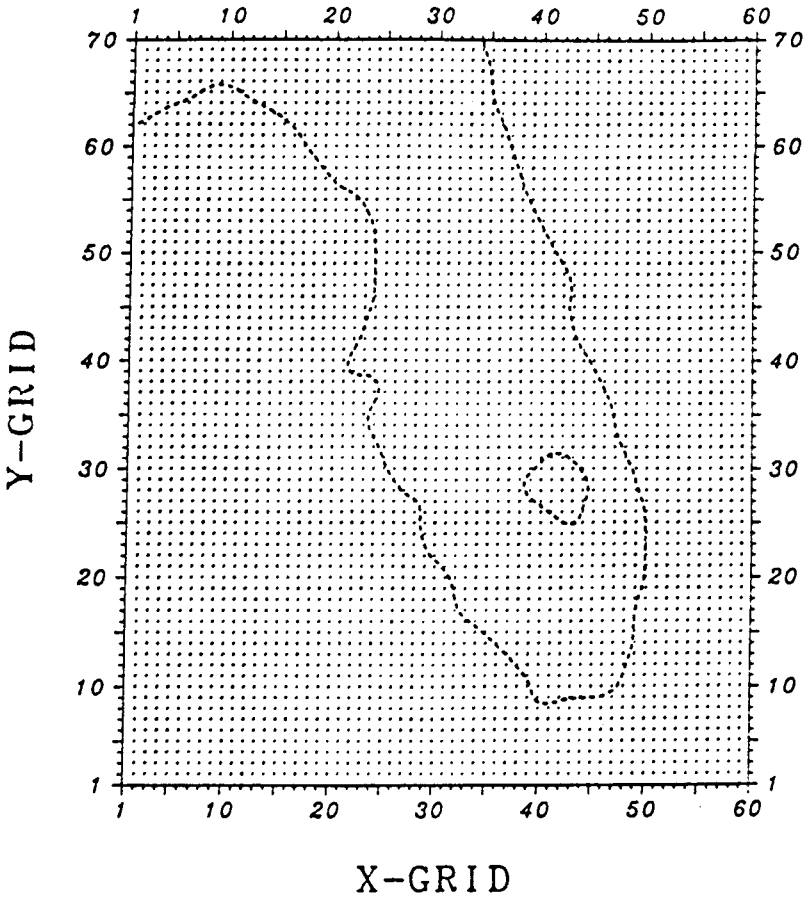

Fig. 1. Outline of the Florida peninsula and model grid.

water. The vertical gradient of the initial potential temperature is assumed to be 4 °C/km.

4. Discussion of Results

4.1. Southeasterly Ambient Wind (Case C1)

A southeasterly flow of 3.5 m s^{-1} ($U_g = -2.5$ m s^{-1} and $V_g = 2.5$ m s^{-1}) is used in this simulation. The wind speed value selected is consistent with climatological observations.

Vectors indicating the predicted horizontal winds (U and V) at 50 m after 3, 7, 11 and 13 h of simulation for the southeasterly ambient wind case are shown in Figure 2. By the third hour after sunrise, the continuous differential heating between land and water and the resulting vertical thermal mixing in the PBL creates a lower pressure region at the surface. For the first few hours of the model

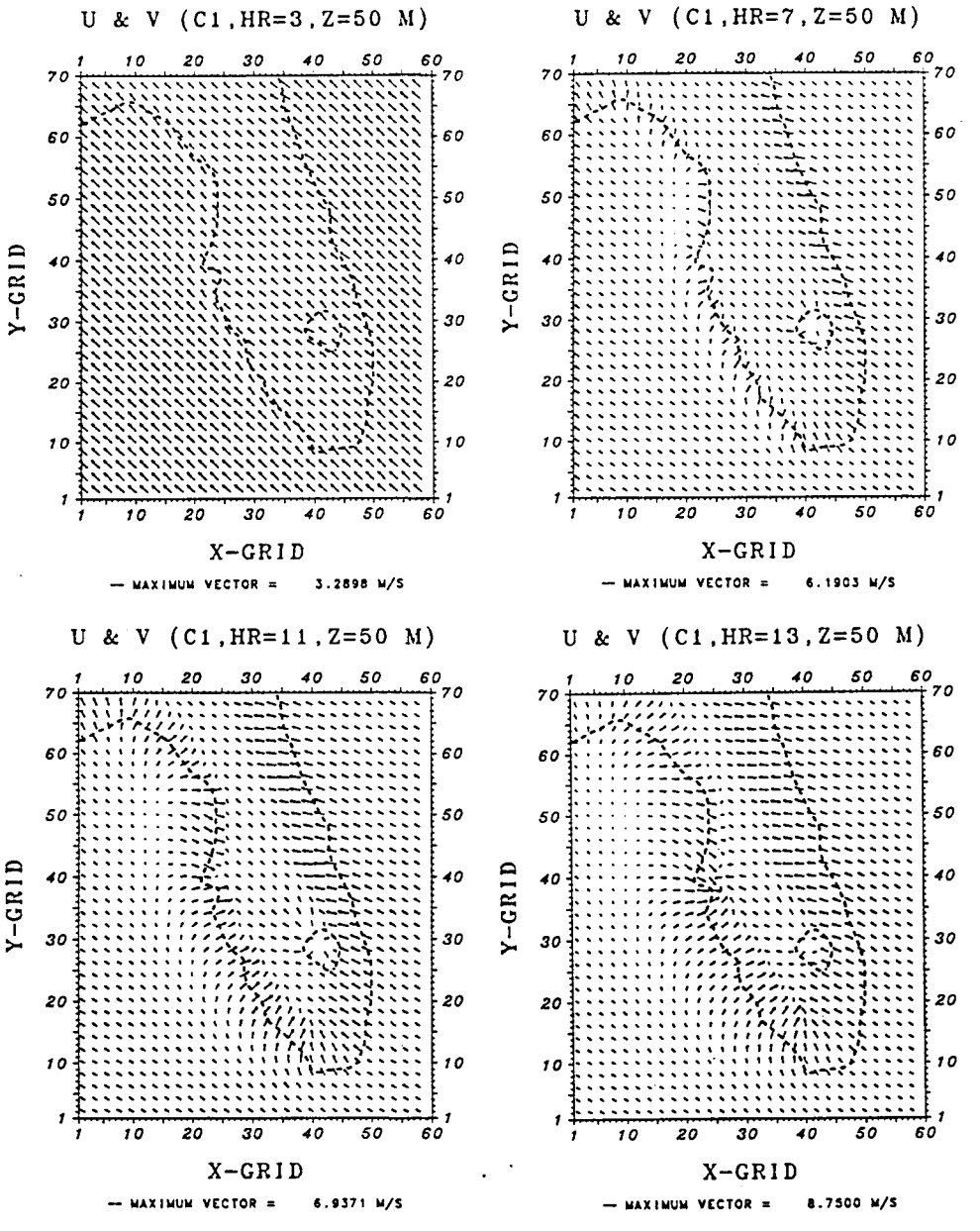

Fig. 2. Vectors indicating the predicted horizontal winds U and V ($m\,s^{-1}$) at 50 m after 3, 7, 11 and 13 h of simulation for the southeasterly ambient wind case.

simulation, the offshore winds near the west coast advect warmer air over the water, causing weak temperature gradients along the west coast, while the onshore winds advect cooler marine air over the land creating strong temperature gradients along the east coast. Therefore, the pressure falls more rapidly along the east

coast and hence the southeasterly winds begin to back earlier along the east coast and later veer along the west coast in response to the pressure falls. By the seventh hour, the winds turn inland along both coasts and increase in speed due to the acceleration of the air towards the lower pressure region. The southeasterly flow becomes nearly westerly along the west coast and easterly along the east coast. Note that the flow is strongly modified by coastal irregularities at this time. The winds propagate inland almost in a direction normal to the coasts. For example, they veer completely from southeasterly to northwesterly at points located northnorthwest of Tampa Bay due to the sharply curved coastline. Thus, mesoscale westerly flow opposing the southeasterly ambient flow causes a well defined and stationary sea breeze primary convergence zone along the west coast. There is also a weaker secondary convergence zone along the east coast caused by the horizontal temperature gradient between the land and the Atlantic ocean. This convergence is not as intense as the one near the west coast because the ambient wind is in the same direction as the local sea breeze. This secondary convergence zone forms earlier than the primary convergence zone, since the pressure gradient caused by the horizontal temperature gradient is largest along the east coast, at least for the first few hours of the simulation.

By the eleventh hour, onshore winds along both the west and the east coasts advect relatively cooler marine air over land. This results in advection of the temperature gradient and hence a convergence zone inland. Inland penetration of the convergence zones are generally controlled by the intensity of the total heat input to the air (Pearson, 1973) and the magnitude of the ambient wind. Wind speeds at the two coasts continue to increase due to the acceleration of the air toward the lower pressure region. By the thirteenth hour, the convergence zone along the east coast moves inland farther as compared to the one along the west coast, since there is no opposing flow along the east coast. The secondary convergence zone obviously moves inland as a function of the magnitude of the ambient wind. However the convergence zone along the west coast shows very little movement due to the opposing ambient flow. The model results also show a landward distortion of the convergence zone produced by Tampa Bay and the sharply curved coastline located to its immediate northnorthwest. Similar results on the modification of sea breeze circulations for irregular coastlines was obtained by McPherson (1970). He concluded that the presence of a bay or other large indentation of a coastline produces a landward distortion of the sea breeze convergence zone.

As shown in Figure 2, lake Okeechobee in south Florida appears to cause its own mesoscale circulation because of its large size. A divergent region over lake Okeechobee is predicted during the integration at least until the end of the eleventh hour of simulation as a result of the lake breeze circulation. For example, the divergent flow over the lake begins to form by the third hour of model integration due to differential heating between the lake and land. A well defined divergent area forms by the seventh and eleventh hours of simulation causing a

cloudless region over the lake during the day and local convergences over south Florida. For example, two local convergence regions caused by the divergent flow of the lake are located north and northwest of the lake by the eleventh and the thirteenth hour of simulation. These local convergences accentuate convective activities at these locations as will be discussed.

Contours of the predicted vertical velocities (W) at 1500 m after 3, 7, 11 and 13 h of simulation for the southeasterly ambient wind case are shown in Figure 3. The results are presented at a typical altitude where maximum vertical velocities had generally their largest values. By the third hour, vertical velocities are predicted along both the coasts, while a subsidence region is apparent over lake Okeechobee. By the seventh hour, a primary and a secondary convergence zone form along the west and the east coast, respectively. In the later stages, the secondary convergence zone which forms earlier than the primary convergence zone along the east coast moves inland, while the primary convergence zone near the west coast over land remains almost stationary. As shown in Figure 3, positive vertical motions occur in the sea breeze convergence zones, while largest vertical velocities occur where the curvature of the coastline is prominent, causing sharp changes in flow direction. For example, the largest upward motion develops over Tampa Bay in response to the effect of distortion of the sea breeze convergence zone caused by coastal irregularities. The local convergence caused by the divergent flow over lake Okeechobee may also have contributed to this maximum upward motion. This process will be examined and presented in detail in Case C3. Another maximum in vertical velocity occurs over the southwestern corner of the peninsula as a result of the mesoscale convergence generated by the sharply curved coastline. During the integration, these two largest maximums are advected northnorthwestward in the general direction of the southeasterly ambient flow and continue to intensify. For example, the one over Tampa Bay reaches a magnitude of about 180 cm s^{-1} by the thirteenth hour, while the corresponding magnitude of the vertical velocity for the other maximum reaches a value of about 85 cm s^{-1}. These regions of strong vertical motion would therefore be the preferred locations for maximum convergence and consequent rainfall and will be discussed later. In contrast, the intensities of the upward motions along the east coast are substantially weaker as compared to those along the west coast. This is due to the fact that the onshore ambient flow is in the same direction as the direction of local acceleration caused by mesoscale convergence with no sharp sea breeze front near the east coast.

To understand the vertical structure of the coastal flow better, a cross-section of wind vectors (u–w) and potential temperatures (θ) across a typical region of strong convection located over Tampa Bay is examined in Figure 4 after 13 h of simulation. The cross-section is a vertical plane (x-z) from west to east. The horizontal gradient of potential temperature shows a well-defined sea-breeze circulation as it moves inland after 13 h of simulation. As can be seen from the figure, there is a strong convergence of the wind over Tampa Bay. These significant

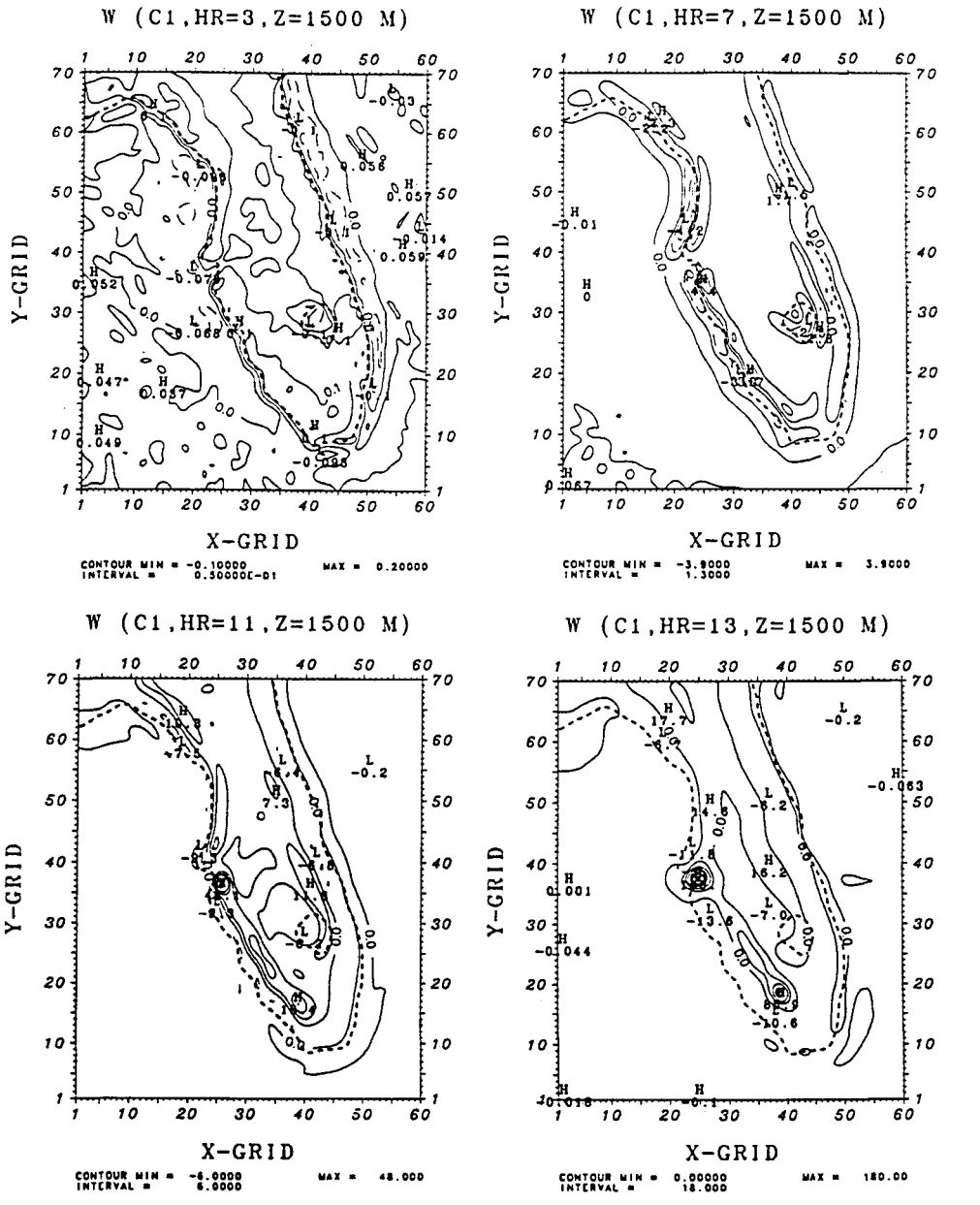

Fig. 3. Contours of the predicted vertical velocity W (cm s^{-1}) at 1500 m after 3, 7, 11 and 13 h of simulation for the southeasterly ambient wind case. The extremes are indicated by letters H (High) and L (Low). Updrafts are represented by solid contours and downdrafts by long dashed contours.

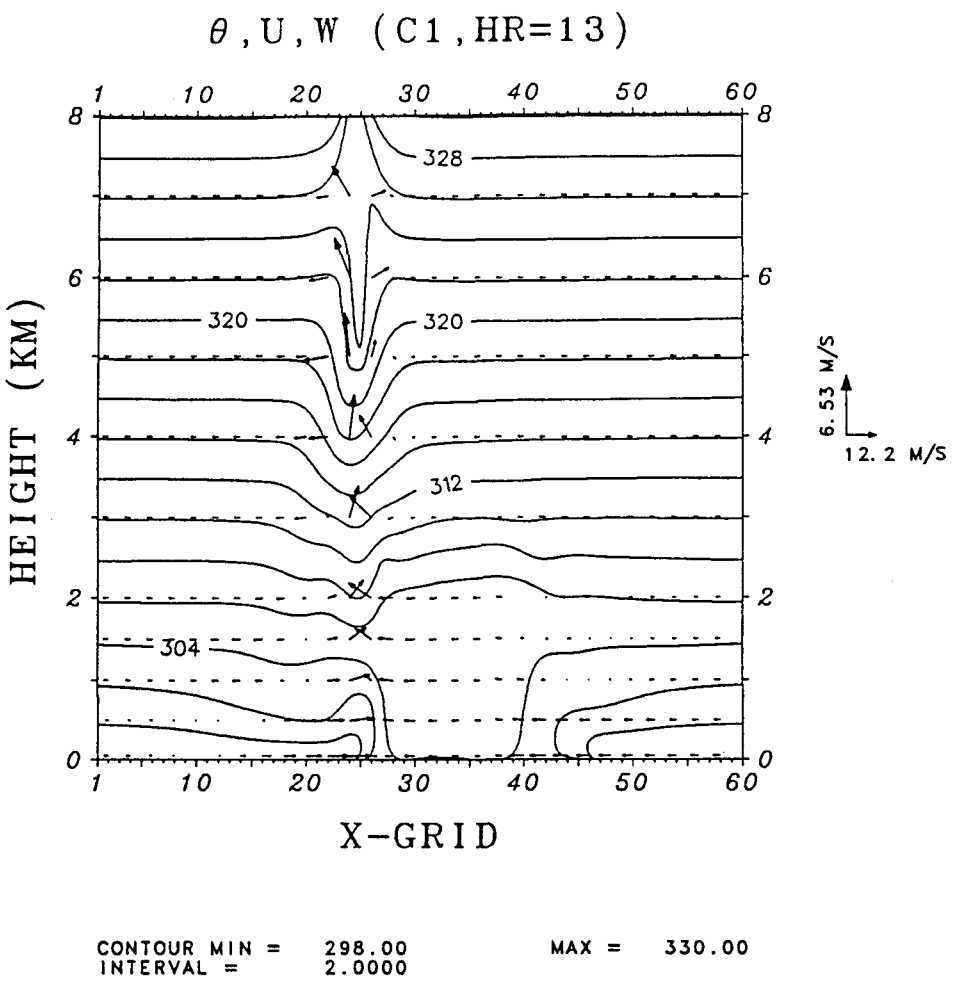

Fig. 4. The vertical cross-section (x-z) of potential temperature (θ) and wind fields (**u**-**w**) at grid point $J = 37$ after 13 h of simulation for the southeasterly ambient wind case. Maximum along-x wind component and vertical velocity are plotted at the right-hand side of the figure. The contour lines represent the potential temperature, while vectors represent the vertical velocity (**w**) and the wind component (**u**) in the x-direction.

updrafts develop over Tampa Bay in response to the effect of distortion of the sea breeze convergence zone caused by coastal irregularities.

The contours of the predicted cloud water (q_c) at 1500 m after 11 and 13 h of simulation for the southeasterly wind case are shown in Figure 5. The results show that there is a good correlation between the development of the sea breeze convergence zones and the formation of the cumulus clouds, as one would expect. In the early morning, cumulus clouds begin to form along both convergence zones (not shown). During the afternoon as the convergence increases, the clouds increase in depth and cloud water content increases. For example, the predicted cloud water reaches its largest magnitude of 68 g kg^{-1}at 2500 m after 11 h of simulation (not shown), while it reaches a value of 102 g kg^{-1} at 5000 m after 13 h

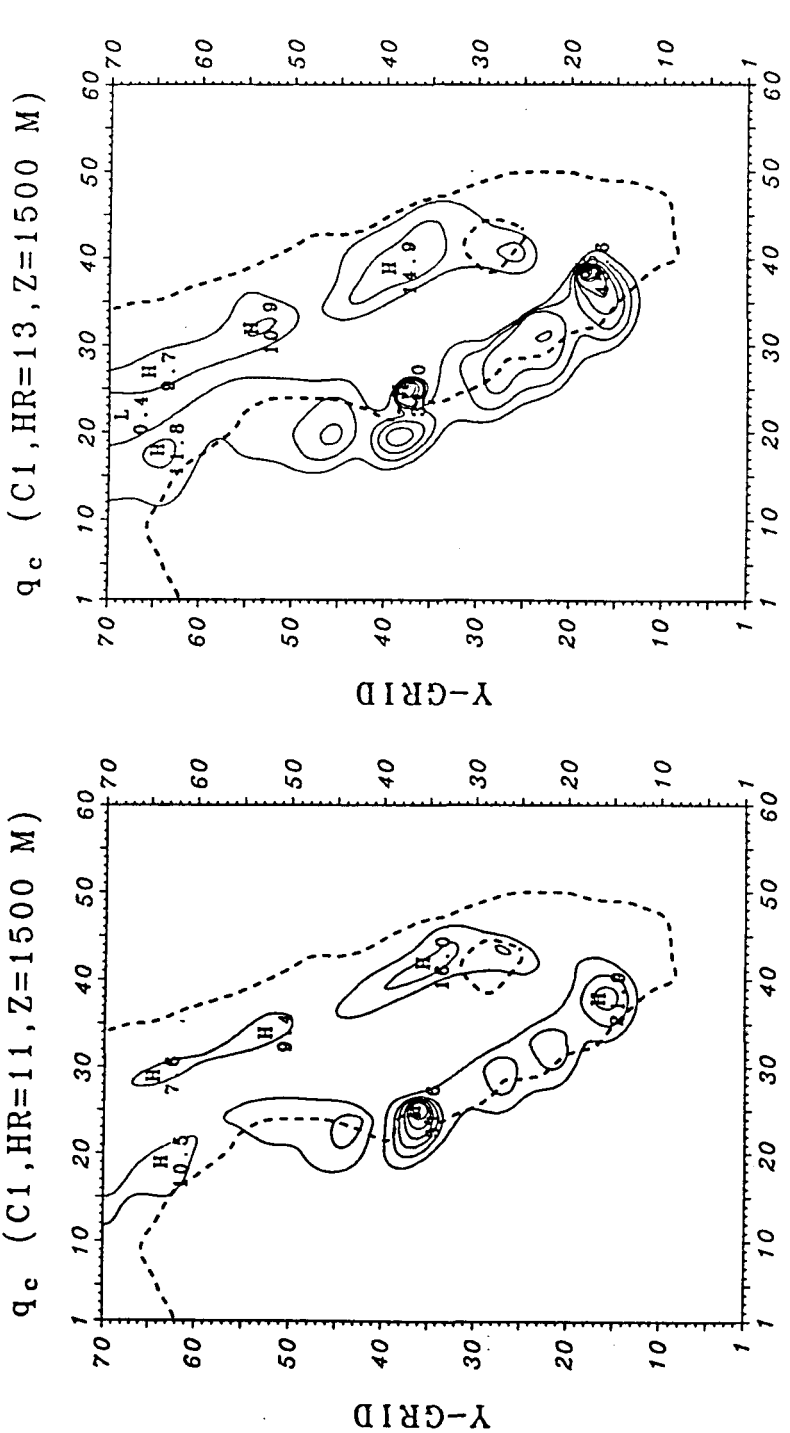

Fig. 5. Contours of predicted cloud water amount q_c (g kg^{-1}) at 1500 m after 11 and 13 of simulation for the southeasterly ambient wind case.

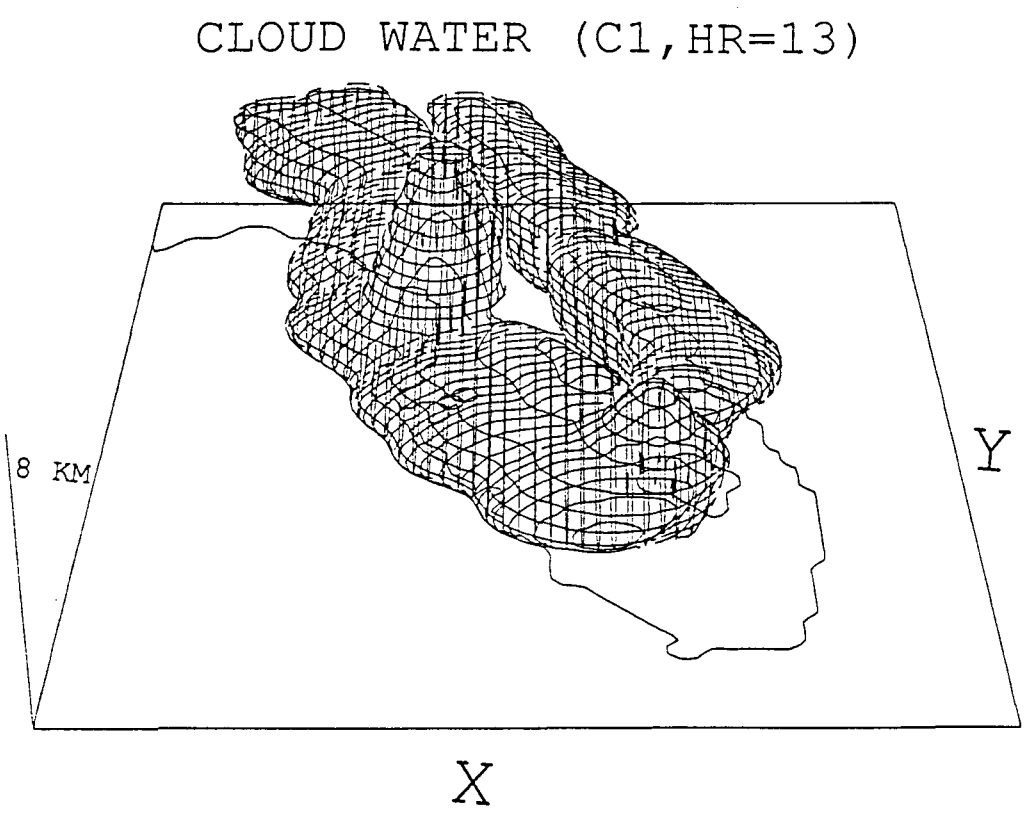

Fig. 6. 3-D plot of the predicted cloud water amount q_c after 13 h of simulation for the southeasterly ambient wind case.

of simulation over Tampa Bay (e.g., see 3-D plot of cloud water after 13 h of simulation for the southeasterly ambient wind in Figure 6) indicating fast growth of the clouds in the afternoons. Most of the deep clouds generally develop along the west coast associated with the strong primary convergence zone, while a weaker cloud band forms along the east coast along the secondary convergence zone. However, not all of the convergence regions lead to precipitation. Deep clouds tend to occur in regions where the curvature of the coastline is prominent, causing sharp turns in the flow direction. For example, maximum values in cloud water at the 1500 m level after 11 and 13 h of simulation are obtained over Tampa Bay due to the curvature of the coastline and over the southwestern corner of the peninsula due to a sharp turn of the flow as shown in Figure 5. Another maximum is also predicted by the model northnorthwest of the lake. This relatively weak maximum is believed to be due to local convergence caused by differential heating between lake and land.

Figure 7 shows predicted cumulative rain water (q_r) at the surface associated with the precipitating clouds after 11 and 13 h of simulation. Significant rain

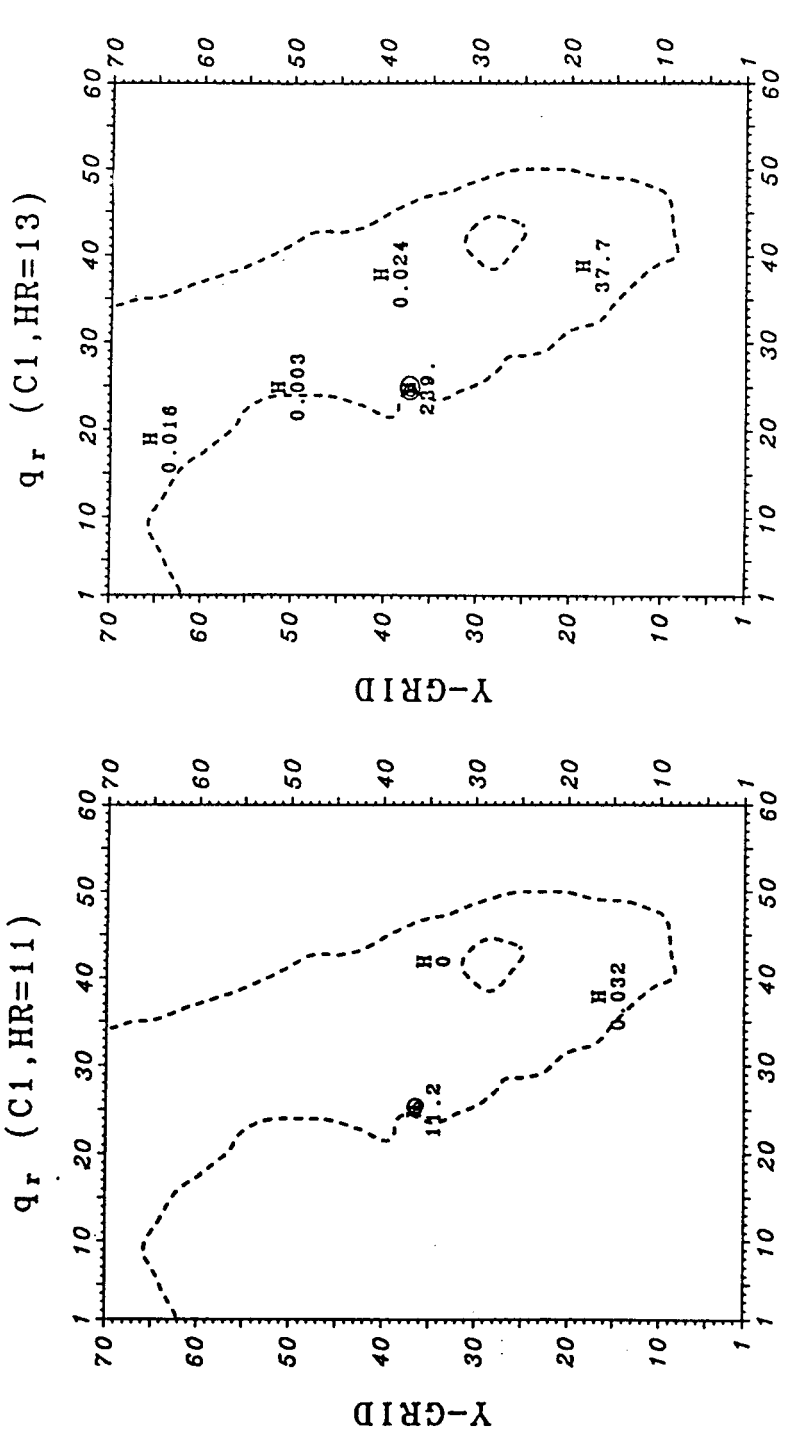

Fig. 7. Contours of the predicted rainfall amount q_r (mm/total hours) at the surface after 11 and 13h of simulation for the southeasterly ambient wind case.

develops over the peninsula only in the afternoon following substantial sea breeze-induced convergence. By the eleventh hour, rainfall that occurs over Tampa Bay and the southwestern corner of the peninsula are consistent with the predicted locations of the intense convection (Figure 5). By the thirteenth hour, heavy rainfall occurs along the primary convergence zone near the west coast of the peninsula. However, heaviest rainfalls occur only over the Tampa Bay area and the southwestern corner of the peninsula with values of about 230 and 38 mm, respectively, by the thirteenth hour. It can also be seen from Figure 7 that weaker cumulus clouds along the secondary convergence zone near the east coast do not produce rain. The rainfall located northnorthwest of the lake must be due to the combined effect of the local convergence caused by the lake breeze and the secondary convergence zone. This will be examined and presented in detail in Case C3.

These results show that most of the intense convection and large rainfall occur in the primary sea breeze convergence zone along the west coast, while weaker cumulus clouds and very little rainfall occur in the secondary sea breeze convergence zone along the east coast under a southeasterly ambient wind. This indicates that sea breeze convergence has a strong influence on convective activities over the Florida peninsula on typical summer days. However, the location and intensity of the convective activities are also affected by local terrain inhomogeneities (such as coastal irregularities).

4.2. Southwesterly Ambient Wind (Case C2)

A southwesterly flow of 3.5 m s^{-1} ($U_g = 2.5$ m s^{-1} and $V_g = 2.5$ m s^{-1}) was used to study the influence of the other dominant wind direction on the sea breeze convergence zone and the convection over the Florida peninsula. All prescribed model parameters were the same as those in Case C1 except wind direction.

Vectors indicating the predicted horizontal winds at 50 m after 3, 7, 11 and 13 h of simulation for the southwesterly ambient wind case are shown in Figure 8. The predicted results appear to have a pattern similar to that found in the earlier case study for a southeasterly ambient wind. The differences are mainly caused by the change in wind direction. In contrast to Case C1, the primary convergence zone is predicted along the east coast rather than along the west coast in response to the southwesterly ambient wind. A weaker secondary convergence zone forms near the west coast earlier than the primary convergence zone. In the later stages of the model integration, the secondary convergence zone moves inland and tends to merge with the stationary primary convergence zone along the east coast. A divergent area over lake Okeechobee is also present for the southwesterly ambient wind case.

Contours of the predicted vertical velocities for the southwesterly ambient wind given in Figure 9 are consistent with the convergence patterns indicated by the horizontal velocities in Figure 8. Early in the morning by the third hour, positive vertical velocity regions along both coasts and a subsidence region over lake

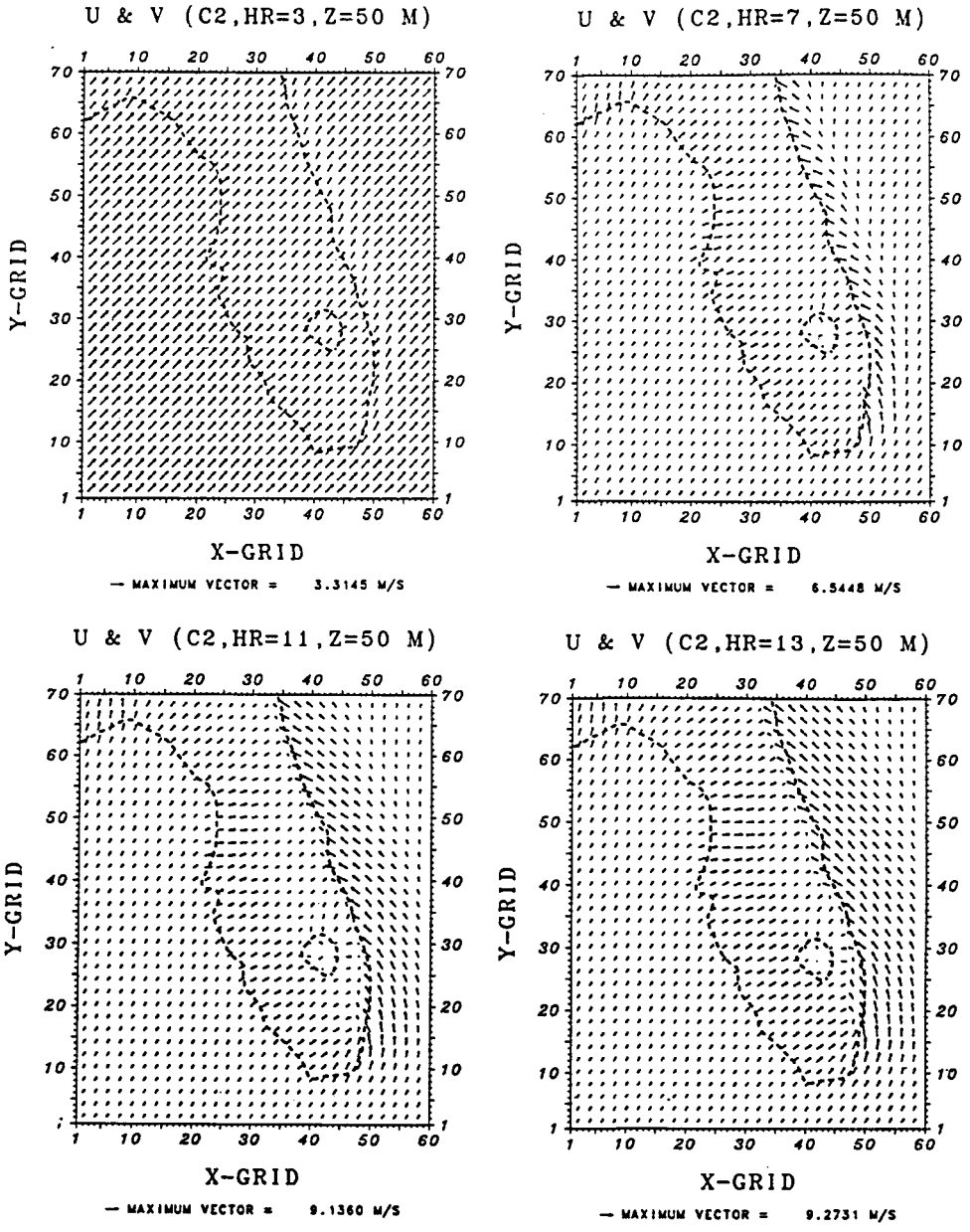

Fig. 8. Vectors indicating the predicted horizontal winds U and V ($m\,s^{-1}$) at 50 m after 3, 7, 11 and 13 h of simulation for the southwesterly ambient wind case.

Okeechobee are apparent. In the afternoon by the seventh hour, intense upward motions develop only along the east coast associated with the primary convergence zone. The subsidence region over the lake also becomes more obvious at this time. Five vertical velocity maxima develop along the east coast at the locations

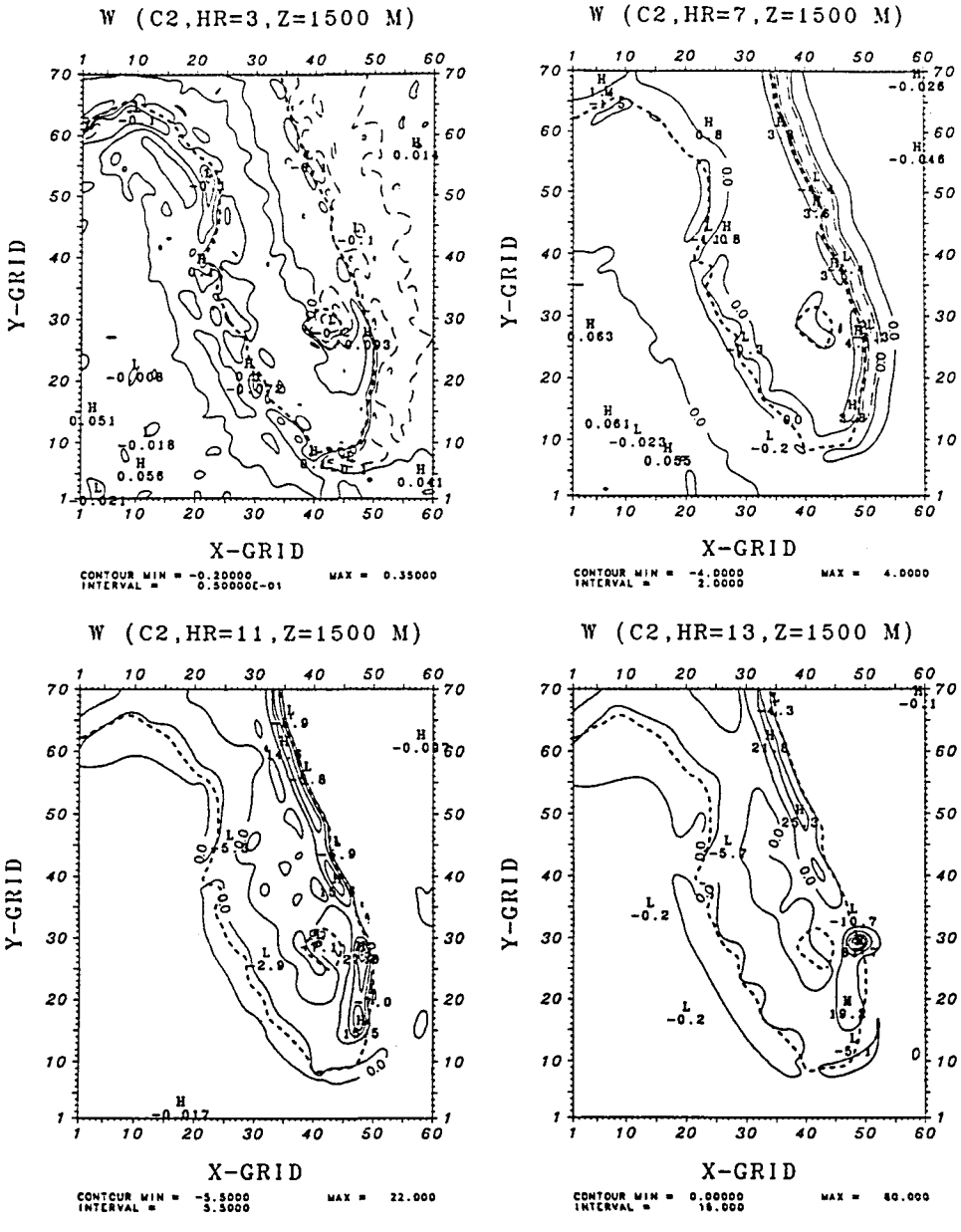

Fig. 9. Contours of the predicted vertical velocity W ($cm\,s^{-1}$) at 1500 m after 3, 7, 11 and 13 h of simulation for the southwesterly ambient wind case. The extremes are indicated by letters H (High) and L (Low). Updrafts are represented by solid contours and downdrafts by long dashed contours

over Miami, east of lake Okeechobee, northeast of the lake and two maxima along the northeastern coast of the peninsula. Note that the largest maximum occurs east of lake Okeechobee. By the eleventh hour, the largest maximum located east of the lake is separated from the one located northeast of the lake. The other maxima along the northeastern coast of the peninsula remain essentially stationary, while the one that developed over Miami moves north in the general direction of the ambient wind. Separation of the two maxima could be due to the influence of the lake breeze; as the lake breeze circulation becomes stronger in the afternoon, the divergent flow over the lake may suppress the convergence zone in this region. By the thirteenth hour, the largest maximum of the predicted vertical velocity located east of the lake reaches a value of 80 cm s^{-1}, while the maximum that formed over Miami moves farther north. The other maxima stay stationary. Obviously, the presence of lake Okeechobee plays an important role on south Florida's mesoscale weather influencing low-level convergence. The lake also contributes to the development of the largest upward motion east of the lake in the southwesterly ambient wind case This largest maximum seems to be due to the combined effect of both the lake breeze and the sea breeze circulations. In order to isolate the effect of the lake under a southwesterly ambient wind, it was decided to conduct a numerical experiment with the lake removed in Case C4.

A comparison of the results from Case C2 with those in Case C1 emphasizes the importance of the influence of coastal irregularities on both sea breeze convergence patterns and the development of convection. The irregular coastline along the west coast appears to influence the magnitudes of the upward motions. For example, the largest magnitude of the predicted maximum vertical velocity in Case C2 is smaller than that found in Case C1. Because irregular coastal shapes along the west coast cause distortion of the sea breezes, they contribute to the development of the largest maximum over Tampa Bay under a southeasterly ambient wind. This indicates that coastal irregularities have an important control mechanism in the development of intense vertical motions and hence convection.

Contours of the predicted cloud water at 1500 m after 11 and 13 h of simulation for the southwesterly wind case are shown in Figure 10. By the eleventh hour, a well developed cloud band associated with the primary convergence zone along the east coast and a weaker cloud band associated with the secondary sea breeze convergence zone near the west coast are prominent. The predicted cloud patterns are consistent with the predicted vertical velocity patterns (Figure 9). As the convergence zone intensifies by the thirteenth hour, deep convection occurs along the east coast. For example, the largest magnitude of cloud water is predicted as 80 g kg^{-1} at 2500 m by this hour (see 3–D plot of cloud water after 13 h of simulation for a southwesterly ambient wind in Figure 11), while it is predicted as 60 g kg^{-1} at 2000 m by the eleventh hour (not shown). Comparison of the results for Case C2 (southwesterly wind) with those for Case C1 (southeasterly wind) indicates that the development of convection in the southeasterly ambient wind case is larger and stronger than that in southwesterly wind case. As discussed

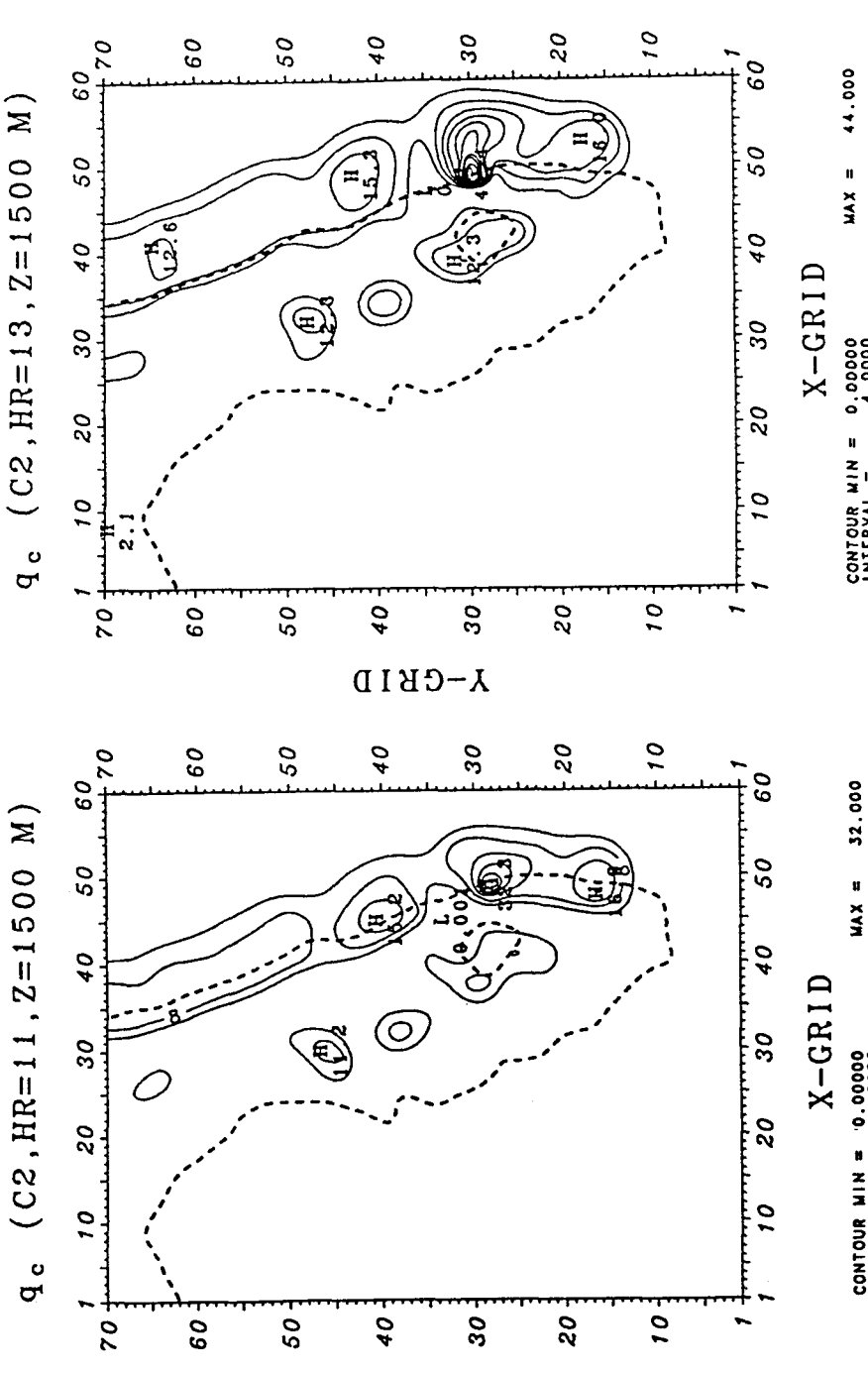

Fig. 10. Contours of the predicted cloud water amount q_c (g kg^{-1}) at 1500 m after 11 and 13 h of simulation for the southwesterly ambient wind case.

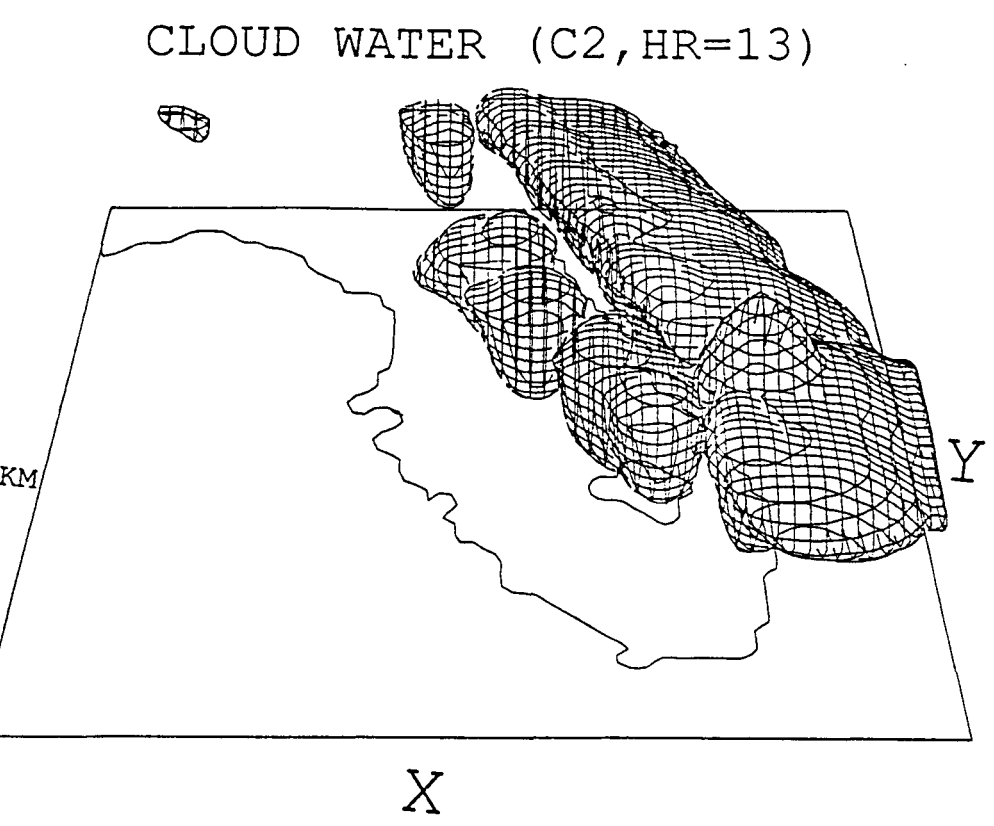

Fig. 11. 3-D plot of the predicted cloud water amount q_c after 13 h of simulation for the southwesterly ambient wind case.

before, the largest amount of cloud water had been predicted to be 102 g kg^{-1} at 5000 m by the thirteenth hour in Case C1. This maximum is due to the combined effect of the quasi-stationary sea breeze front along the west coast, the lake breeze and the coastal irregularities of the west coast.

Figure 12 shows the predicted cumulative rain water at the surface after 11 and 13 h of simulation. By the eleventh hour, rainfall occurs only at a location east of the lake associated with the strong upward motion shown in Figure 9. However, by the thirteenth hour, significant rain develops after the intensification of the primary sea breeze convergence zone along the east coast. No rain is predicted by the model along the secondary convergence zone. Comparison of the results for Case C2 with those for Case C1 shows that the magnitudes and the number of maximums of the predicted rainfalls are less than those predicted for Case C2 due to a smoother coastline along the east coast.

It is clear from a comparison between the two case studies that the spatial and temporal variations of the predicted sea breeze patterns and hence the convective activities are strongly influenced by the ambient wind direction over the Florida

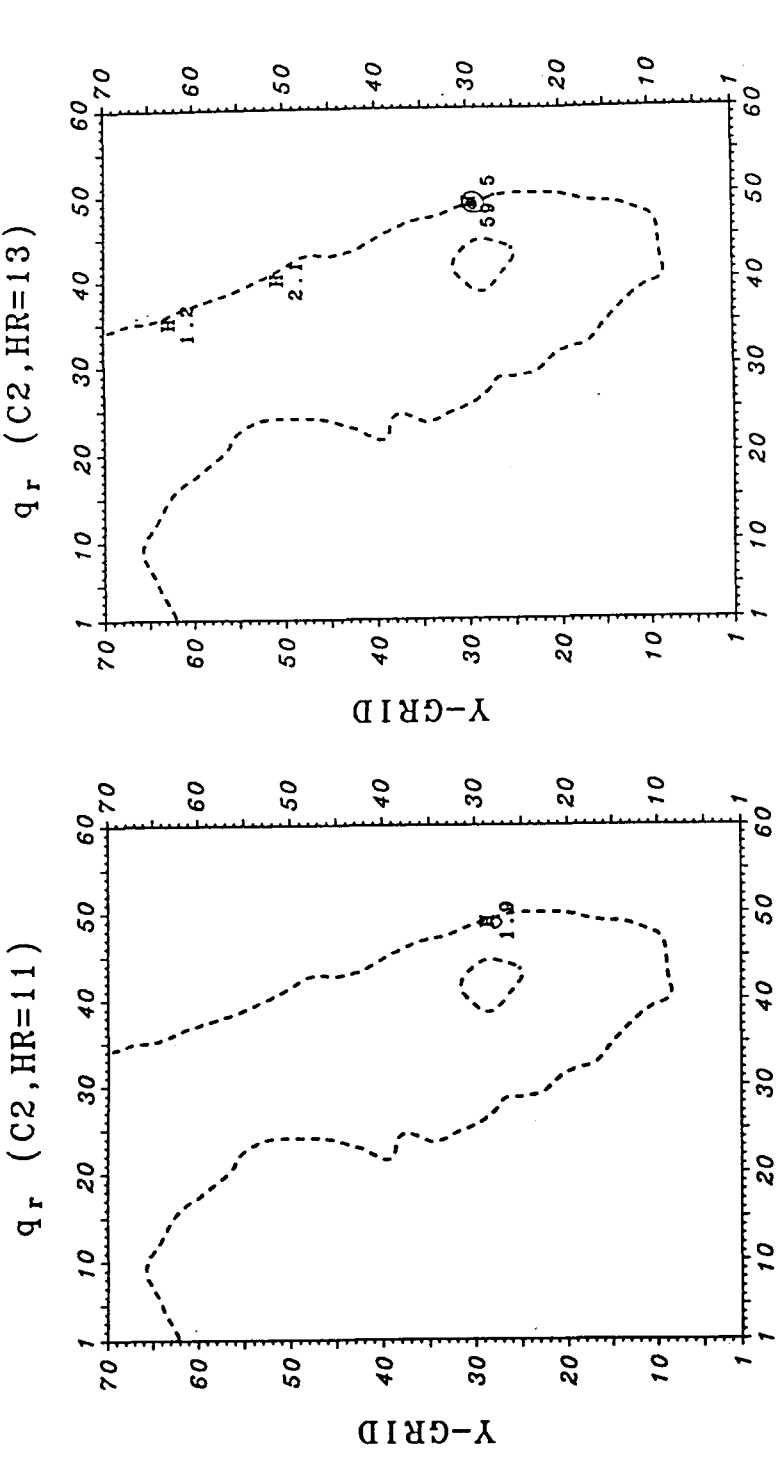

Fig. 12. Contours of the predicted rainfall amount q_r (mm/total hours) at the surface after 11 and 13 h of simulation for the southwesterly ambient wind case.

peninsula on typical summer days. Under a southeasterly ambient wind, the primary convergence zone forms along the west coast resulting in the development of cumulus clouds early in the day. In the afternoon, continuous heating of the land and the strength of the sea breeze aid in the development of deep convection, causing heavy rain along the west coast. Under a southwesterly ambient wind, the primary convergence zone forms along the east coast of the peninsula resulting in the development of strong convection and heavy rain along the east coast late in the afternoon. Results for both cases have also suggested that the presence of lake Okeechobee is an important geographical feature. Lake Okeechobee appears to play an important role on the mesoscale weather of southern Florida. Predicted features in these two case studies are consistent with observations over the Florida peninsula (e.g., see Pielke, 1974; Pielke and Mahrer, 1978; Frank *et al.*, 1967).

4.3. Influence of Lake Okeechobee under southeasterly wind (Case C3)

The previous case studies indicate that lake Okeechobee is an important feature affecting mesoscale weather in south Florida. In order to examine the influence of the lake on south Florida's mesoscale weather under southeasterly ambient winds, the prescribed parameters in the model are kept identical to those in Case C1 except for the removal of the lake from the model domain.

Figure 13 shows the predicted vertical velocities at 1500 m after 3, 7, 11 and 13 h of simulation for the southeasterly ambient wind case without the lake. Although the predicted sea breeze patterns are generally the same as in Case C1, substantial differences occur in the predicted vertical velocities between the results of Case C1 and Case C3 in the vicinity of the lake. For example, the vertical motion that occurs over Tampa Bay is smaller in Case C3 than that found in Case C1. The maximum value of the vertical velocity in this region is about 120 cm s^{-1} by the thirteenth hour, while for Case C1 the corresponding maximum value was about 180 cm s^{-1}. Obviously, when the lake effect is included, the presence of the lake breeze generates greater convergence in this region. Another major difference between the two cases occurs east of the lake. In Case C1, a maximum in vertical motion forms east of the lake by the seventh hour (Figure 3). This cell splits into two by the eleventh hour. By the thirteenth hour, one of these maxima moves to a location northwest of the lake in the general direction of the ambient wind, while the other shows little movement. Although a maximum vertical velocity at a location east of where the lake would have been is still predicted in Case C3, the magnitude of this maximum is now smaller than that found in Case C1. And also during the integration, the maximum maintains its identity and does not split. This is not quite apparent in Figure 13 because of the coarse contour intervals. It therefore appears that the cooling effect of the lake breeze in Case C1 causes separation of this cell in this region.

Comparison of the predicted rain water between Case C1 (Figure 7) and Case C3 (Figure 14) for a southeasterly ambient wind also shows the influence of lake Okeechobee on south Florida's mesoscale weather. The magnitudes of the

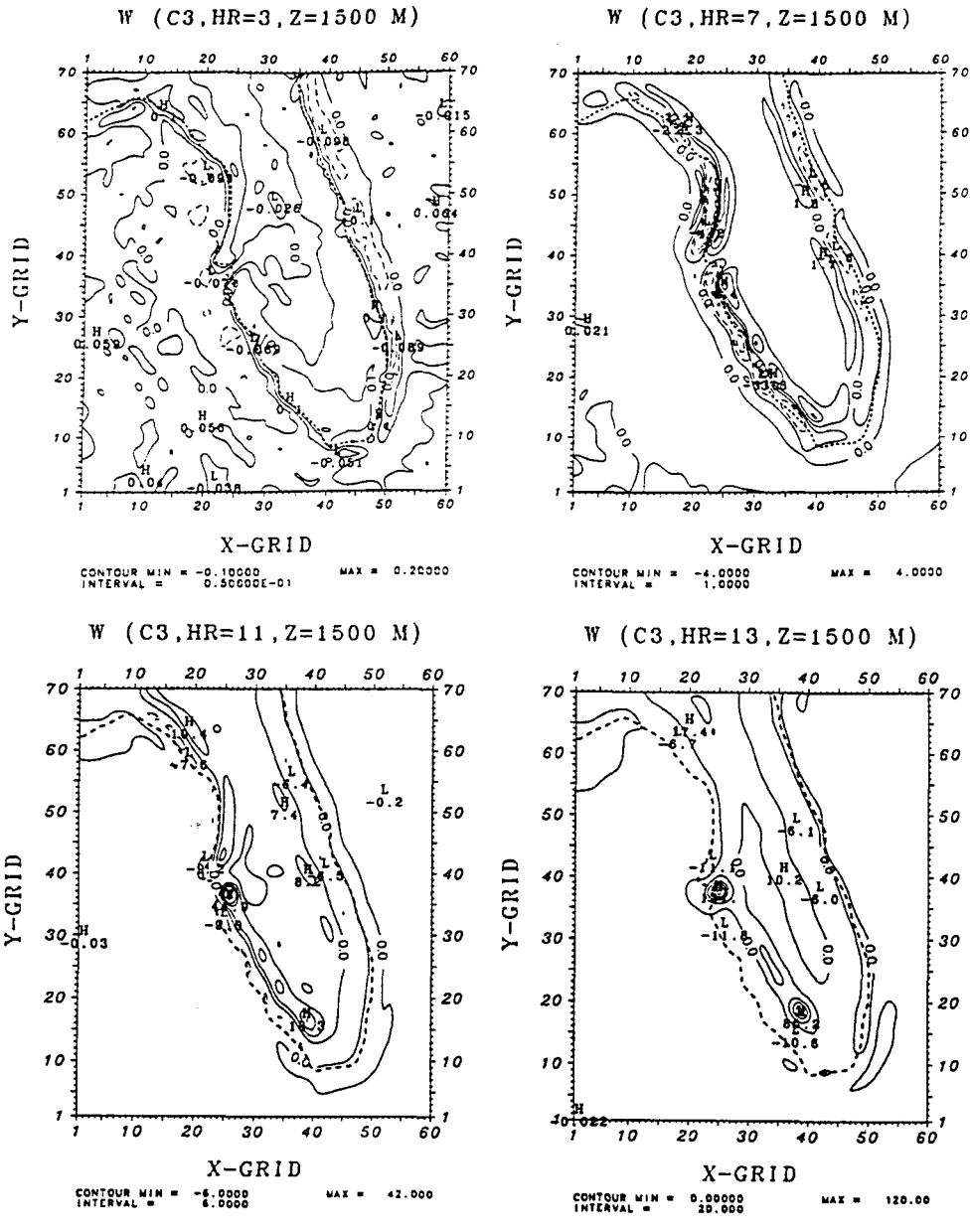

Fig. 13. Contours of the predicted vertical velocity W (cm s^{-1}) at 1500 m after 3, 7, 11 and 13 h of simulation for the southeasterly ambient wind case, but lake Okeechobee is removed. The extremes are indicated by letters H (High) and L (Low). Updrafts are represented by solid contours and downdrafts by long dashed contours.

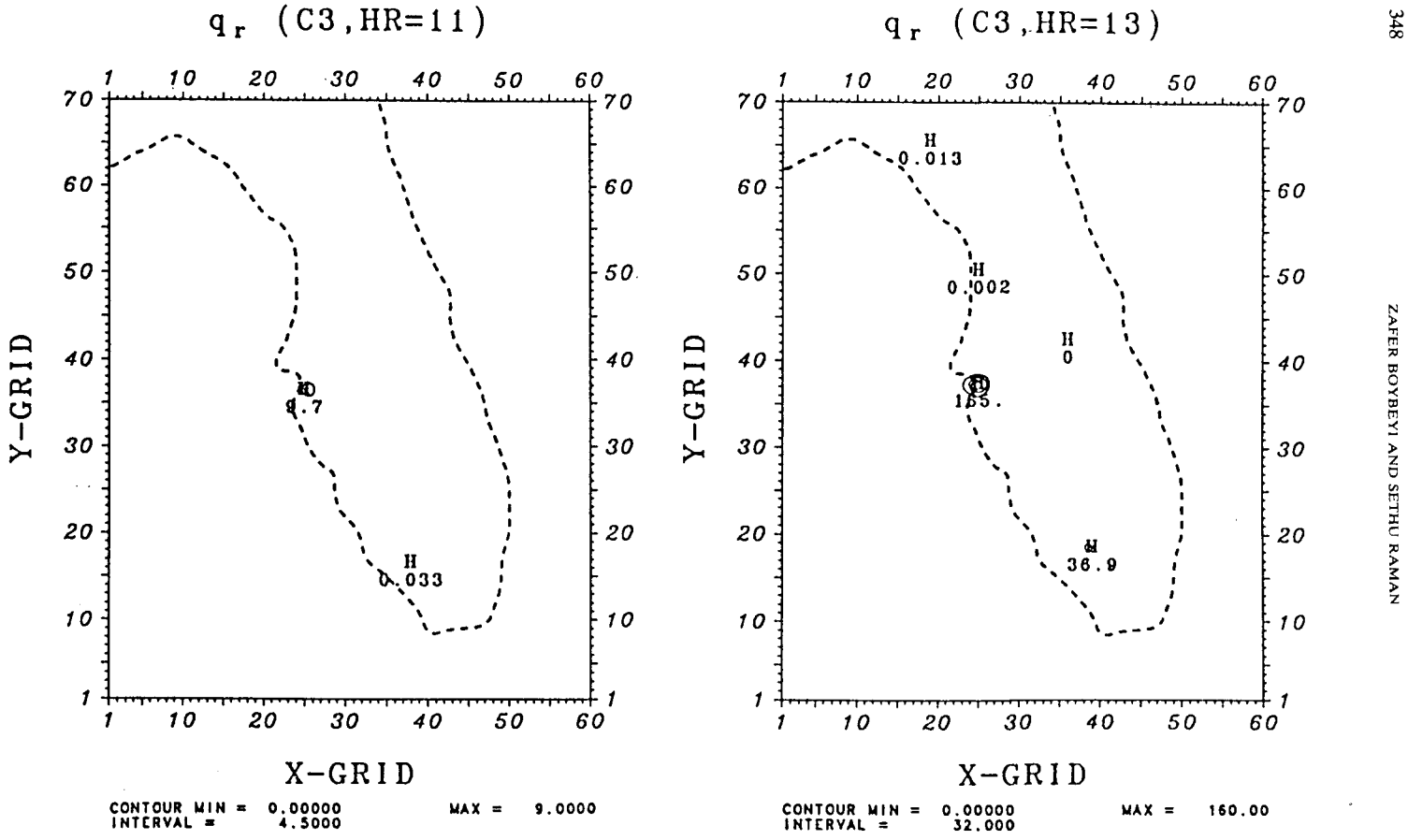

Fig. 14. Contours of the predicted rainfall amount q_r (mm/total hours) at the surface after 11 and 13 h of simulation for the southeasterly ambient wind case, but lake Okeechobee is removed.

predicted rainfall located over Tampa Bay is smaller in Case C3 than that in Case C1, while the rainfall located northnorthwestward of the lake in Case C1 is not present in Case C3. Presence of the lake breeze in Case C1 obviously generates more convergence in these regions and hence produces larger rainfalls. The magnitude of other maxima are essentially the same.

4.4. Influence of lake Okeechobee under southwesterly wind (Case C4)

The influence of lake Okeechobee on south Florida's mesoscale weather under the other dominant ambient wind direction is examined in this case. All the prescribed parameters are kept identical to those in Case C2 except that the lake is removed from the model domain. Figure 15 shows the predicted vertical velocities at 1500 m after 3, 7, 11 and 13 h of simulation for a southwesterly ambient wind without the lake. Although the predicted sea breeze patterns (Figure 15) are generally the same as those in Case C2, differences occur in the predicted vertical velocities between the two cases. The largest vertical motion that was east of the lake for Case C2 is not present. Nevertheless, a relative maximum in vertical velocity still forms east of where the lake was. However, the magnitude of this maximum is smaller than that predicted in Case C2. For example, by the thirteenth hour, the magnitude of the vertical velocity in this region is predicted to be about 25 cm s^{-1}, while in Case C2 the maximum value was about 80 cm s^{-1} at equivalent time. Existence of the maximum vertical motion in this location even without the lake shows the importance of sharp turns of the flow due to the curvature of the coast in this region. When the lake is included, a larger vertical motion is generated (Case C2). Obviously, the intense convection that formed east of the lake in Case C2 is due to the combined effect of the lake breeze and sea breeze circulations. Another difference that occurs between the two cases is that separation of the two maximums located east and northeast of the lake after hour 11 in Case C2 does not occur in this case. This is believed to be due to the fact that the cooling nature of the lake breeze is not present in this case to suppress convergence. Magnitudes and the locations of the other maximums located along the northeastern coast of the peninsula remain essentially the same. The differences between the two cases occur only in the region adjacent to the lake. This indicates that the influence of lake Okeechobee is felt only in south Florida's mesoscale weather.

The predicted rainfall amount at the surface after 11 and 13 h of simulation shown in Figure 16 also emphasizes the importance of the lake for south Florida. The results show that temporal and spatial variations of the rainfall associated with the predicted cumulus clouds are strongly modified by the presence of lake Okeechobee. In contrast to Case C2, rain is not produced at least until the end of the eleventh hour of simulation in the absence of the lake. By the thirteenth hour, the predicted rainfall pattern in south Florida is obviously different from that predicted in Case C2. For example, the largest rainfall predicted east of the lake in Case C2 was about 57 mm by the thirteenth hour. Although this maximum is still predicted in approximately the same location, the rainfall amount is now

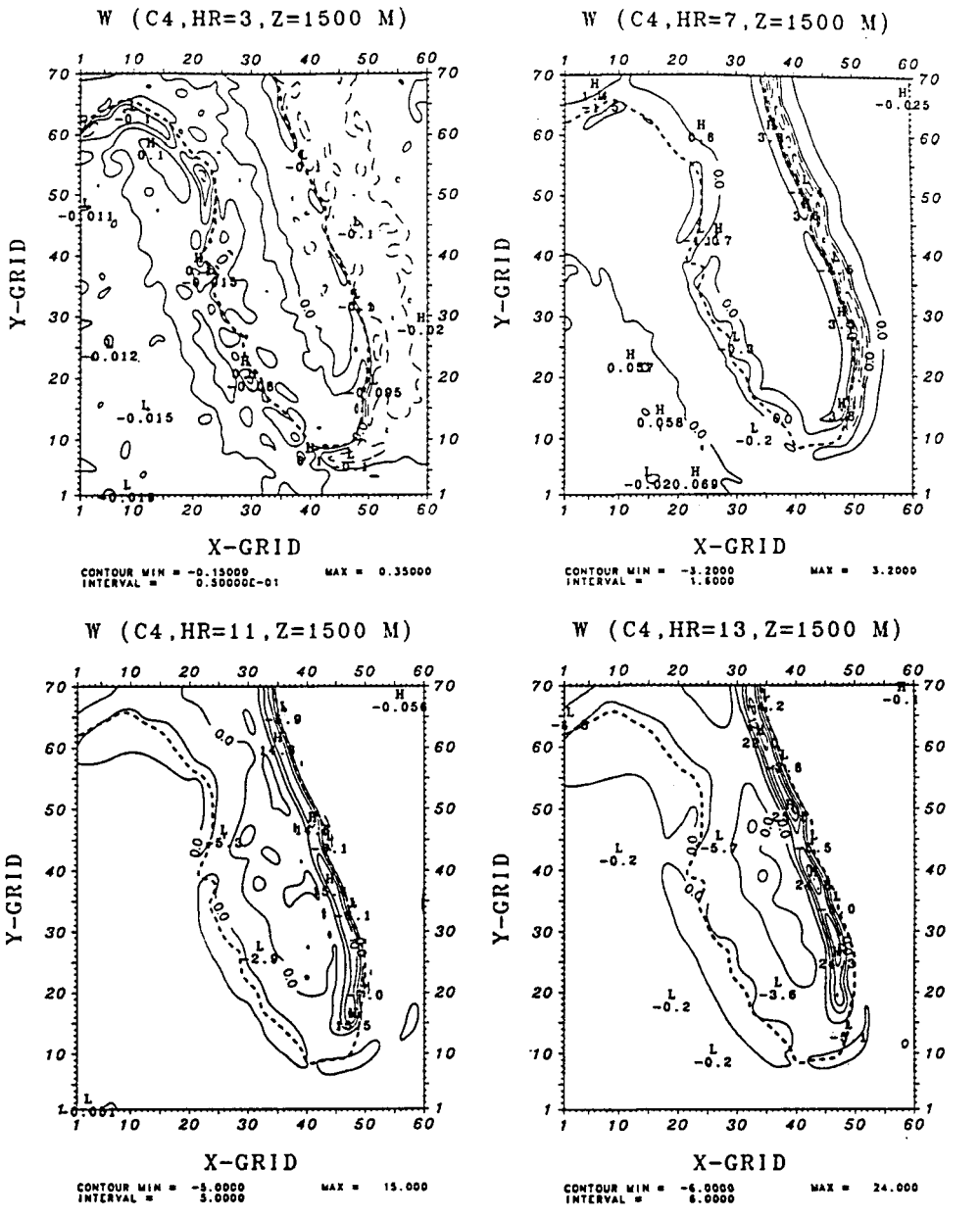

Fig. 15. Contours of the predicted vertical velocity W (cm s^{-1}) at 1500 m after 3, 7, 11 and 13 h of simulation for the southwesterly ambient wind case, but lake Okeechobee is removed. The extremes are indicated by letters H (High) and L (Low). Updrafts are represented by solid contours and downdrafts by long dashed contours.

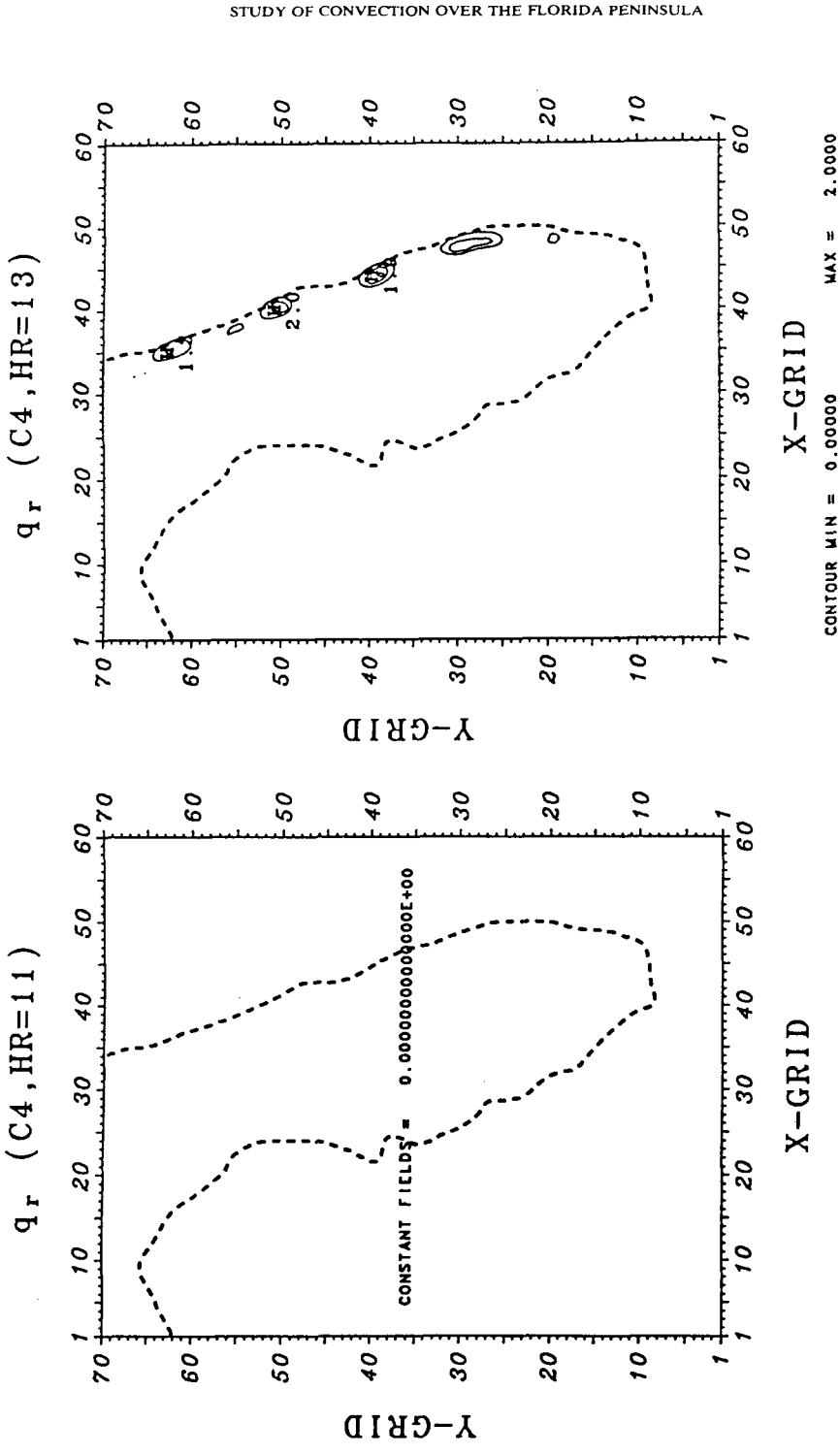

Fig. 16. Contours of the predicted rainfall amount q_r (mm/total hours) at the surface after 11 and 13 h of simulation for the southwesterly ambient wind case, but lake Okeechobee is removed.

much smaller (2 mm) than that found in Case C2. On the other hand, two more shower areas are created in south Florida by the removal of the lake in Case C4. Magnitude and location of the other two predicted maximums located near the northeastern coast of the peninsula remain essentially the same in both cases. It therefore appears that temporal and spatial variations in convection in south Florida are highly influenced by the presence of the lake.

4.5. Influence of Surface Roughness (Case C5)

The relative importance of differential surface roughness on mesoscale circulations over the peninsula is examined in this case. Values of all the prescribed model parameters are set identical to those in Case C2 (southwesterly ambient wind case) except that the surface roughness lengths over land and water are assumed initially to be equal to 0.0015 cm. Then, their values are calculated both over the land and the water by using the Charnock's relationship given by

$$z_0 = 0.018 \frac{u_*^2}{g}$$

where u_* is friction velocity and g is gravity. Hence, spatial variation of surface roughness between land and water is ignored. Note that surface roughness values were assumed to be 4 cm over land, while Charnock's relationship given above was used over the water in Case C2.

The predicted vertical velocities at 1500 m after 3, 7, 11 and 13 h of simulation for Case C5 are given in Figure 17. A comparison of the results between Cases C2 and C5 shows significant differences in the magnitudes of vertical motions. The magnitudes in Case C5 are predicted to be smaller than those in Case C2 at least until the end of the seventh hour of simulation (Figure 17). For example, magnitude of the vertical velocity reaches a value of about 2 cm s^{-1} by the seventh hour of simulation in Case C5, while it has a value of 4 cm s^{-1} at equivalent time in Case C2. This must be due to the larger surface roughness values over land in Case C2. The larger surface roughness values generate more intense vertical mixing of heat early in the day as compared to Case C5 as surface heating increases. Turbulent transfer and vertical convection caused by the vertical mixing of heat now carry a larger amount of heat upward with the consequence that the air over the rough land is warmer than over a smoother land surface. This causes the temperature difference between the land and the water to intensify, causing the pressure to fall more rapidly over the peninsula. Therefore, the vertical velocities in Case C2 at least for the first seven hours of simulation are larger than those in Case C5 in response to the rapid pressure fall caused by larger surface roughness values. However, the predicted vertical velocity values in Case C5 generally become larger than those in Case C2 later in the day (afternoon). For example, the magnitude of the vertical velocity reaches a value of about 95 cm s^{-1} at the thirteenth hour of simulation in Case C5, while it has a value of 80 cm s^{-1} at

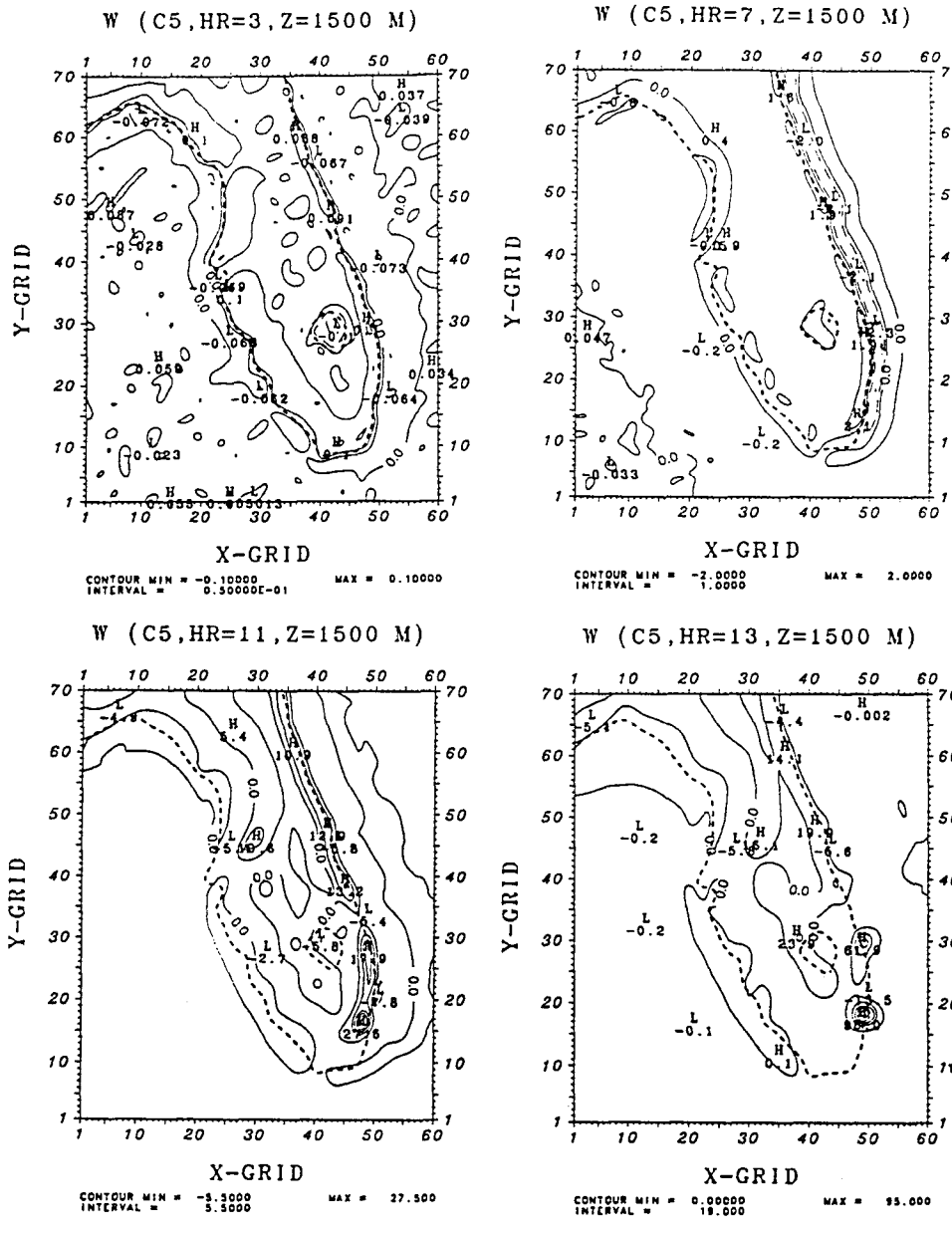

Fig. 17. Contours of the predicted vertical velocity W (cm s^{-1}) at 1500 m after 3, 7, 11 and 13 h of simulation for the southwesterly ambient wind case, but no differential roughness. The extremes are indicated by letters H (High) and L (Low). Updrafts are represented by solid contours and downdrafts by long dashed contours.

equivalent time in Case C2. This must be due to the fact that the larger surface roughness values in Case C2 retard the low level winds in the afternoon as surface heating decreases. This causes less intense convergence in Case C2 and hence generates smaller vertical velocities in Case C2 as compared to Case C5 in the afternoon.

Contours of the predicted rain water for Case C5 at the surface after 11 and 13 h of simulation are shown in Figure 18. Location and magnitude of the rainfalls associated with the convergence patterns indicated by vertical velocities shown in Figure 17 are different than those predicted in Case C2. Also, the magnitudes of the predicted rainfall are generally larger in Case C5 than those in Case C2 afternoon at equivalent times. On the other hand, location of the largest rainfall maximum shifts towards Miami in Case C5 by the eleventh hour and the number of maximums increases by the thirteenth hour. The results presented here indicate that surface roughness values over land appear to influence the location and the magnitude of the convective activities by determining the intensity of the vertical turbulent transport of heat and momentum.

4.6. Light Ambient Wind (Case C6)

Convective activity associated with a sea breeze convergence zone under light ambient wind conditions is examined in this case using a light southwesterly ambient wind. (Light winds are also often observed over the Florida peninsula in addition to southeasterly and southwesterly wind conditions.) All of the model parameters are set equal to those in Case C2 except that calm winds are assumed ($U_g = 0.1\,\mathrm{m\,s^{-1}}$ and $V_g = 0.1\,\mathrm{m\,s^{-1}}$).

The predicted horizontal wind (U and V) at 50 m, vertical velocity (W) at 1500 m, cloud water (q_c) at 1500 m and rain water (q_r) at the surface after 11 h of simulation are shown in Figure 19. The results are presented only for the eleventh hour of simulation for brevity. In contrast to the southeasterly and southwesterly ambient wind cases, the results show that the predicted patterns on both the west and the east coasts are about the same, and remain almost stationary during the day. This is in agreement with observations (Frank *et al.*, 1967). Figure 19a shows that the sea breeze convergence zone occurs along the entire coastline of the peninsula. In addition, a subsidence region is present over lake Okeechobee. The winds propagate inland in a direction normal to the coasts and increase in speed due to the acceleration of the air toward lower pressure. Note that the wind speed is larger along the coastlines than anywhere else. The convergence zones and the subsidence region remain almost stationary and show little movement during the day (not shown). The strongest convergence occurs over the southern tip of the peninsula, because the winds converge from offshore directions. Model results reveal upward motions (Figure 19b) almost parallel to the coasts, with maximums where coastal irregularities are greatest and where sharp turns of the flow occur. For example, the largest upward motions are predicted near the southern tip of the peninsula due to the sharp turn of the flow, and east of lake

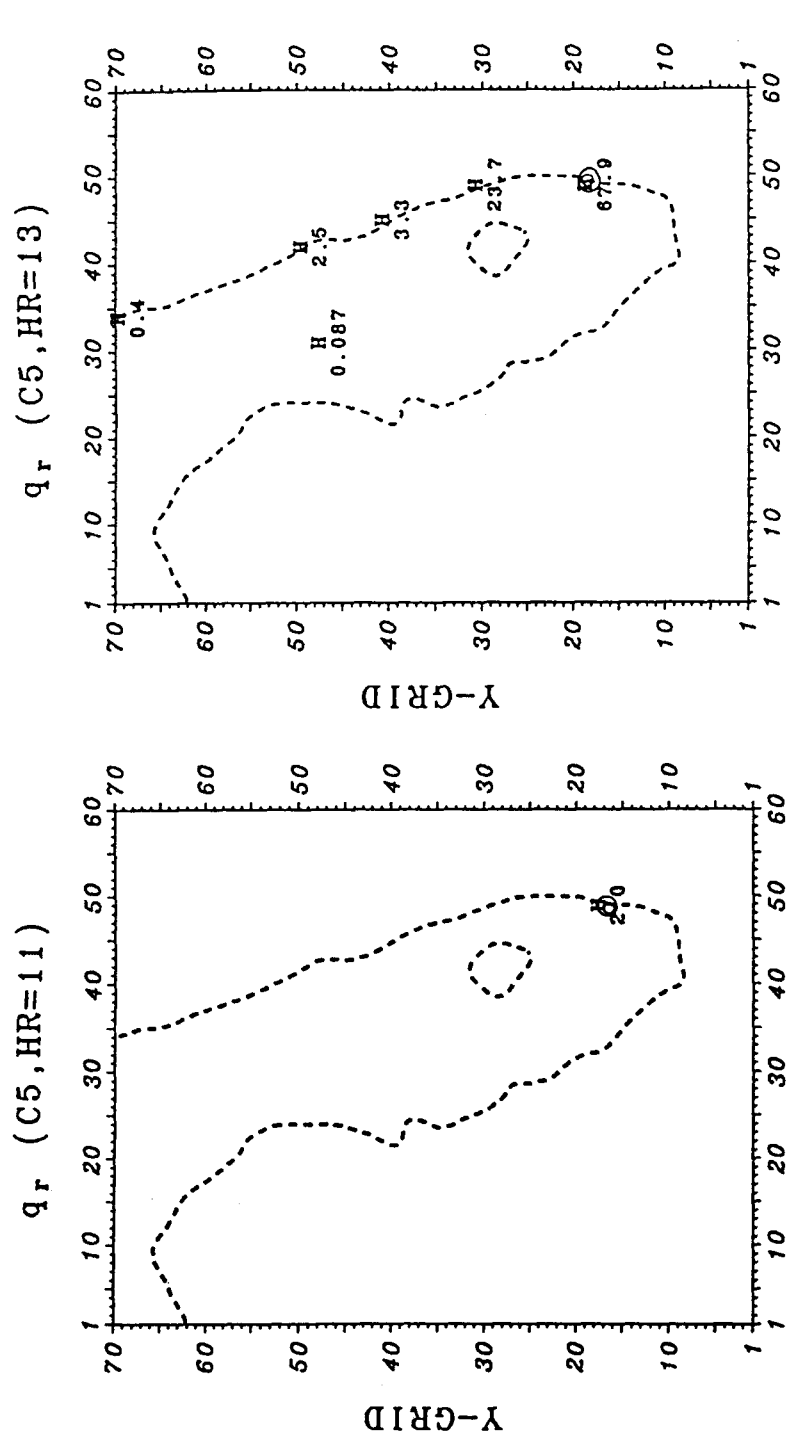

Fig. 18. Contours of the predicted rainfall amount q_r (mm/total hours) at the surface after 11 and 13 h of simulation for the southwesterly ambient wind case, but no differential roughness.

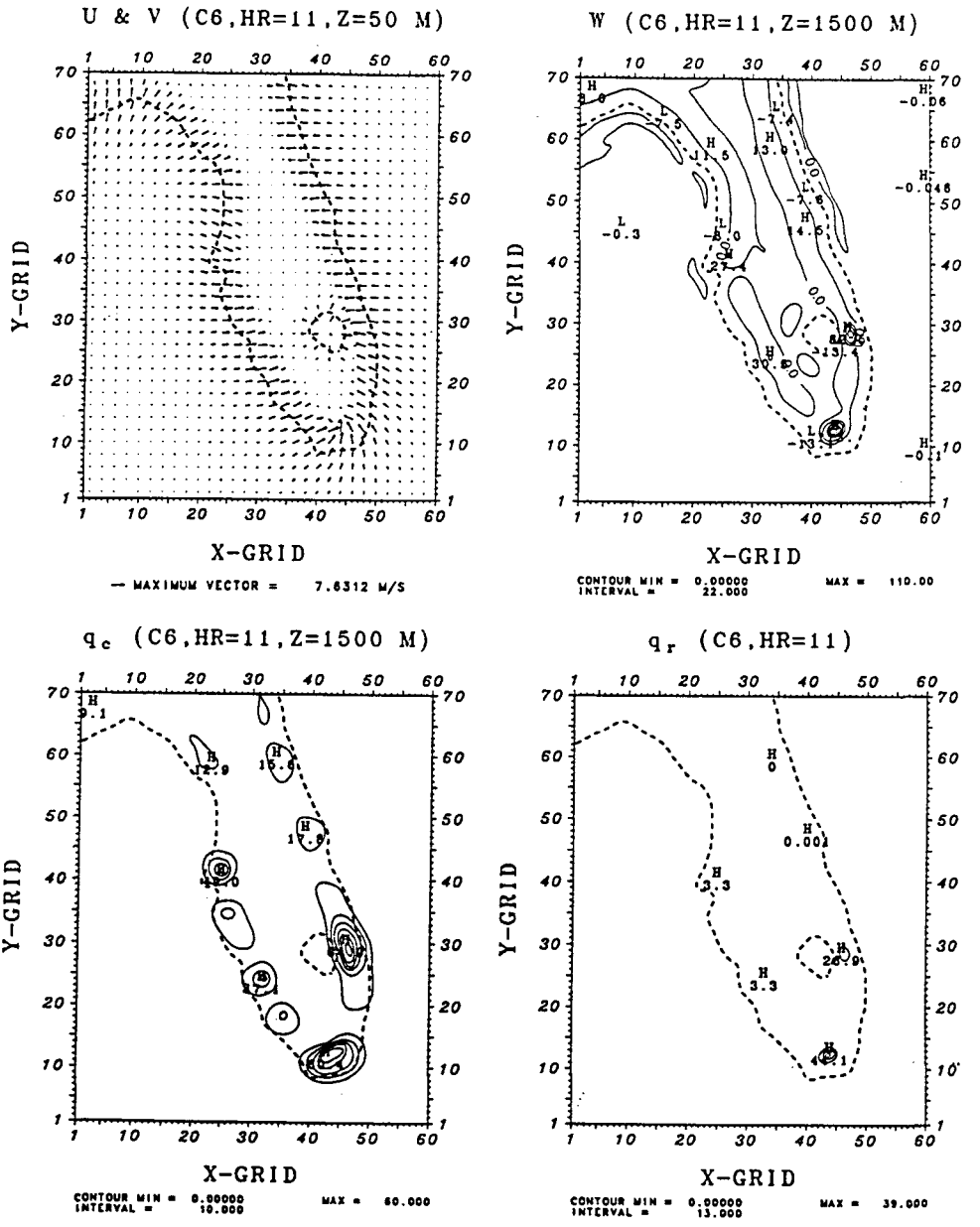

Fig. 19. Vectors indicating the predicted horizontal winds U and V ($m\,s^{-1}$) at 50 m, contours of the predicted vertical velocity W ($cm\,s^{-1}$) at 1500 m, contours of the predicted cloud water q_c ($g\,kg^{-1}$) at 1500 m and contours of the rainfall amount q_r (mm/total hour) at the surface after 11 h of simulation for the light southwesterly ambient wind case.

Okeechobee due to the combined effect of the sea and lake breezes. The predicted cloud pattern associated with the convergence zones shows similar behavior aligning parallel to the coasts (Figure 19c). Huge cumulus clouds (reaching almost to the top of the model) develop over the southern tip of the peninsula east of the lake and over Tampa Bay in the afternoon associated with intense upward motions producing the largest rainfalls in these regions (Figure 19d). The cloud bands aligned parallel to the coasts also produce rain close to the coastlines of the peninsula (Figure 19d) during the afternoons. The largest rainfalls occur over the southern tip of the peninsula and east of the lake.

A comparison of the results for the predicted variables (u, v, w, q_c, and q_r) in Figure 19 with those for Cases C1 and C2 at equivalent times shows that the magnitudes of all the predicted variables in Case C6 are larger than those found in Cases C1 and C2. This is due to the fact that stronger ambient winds in Cases C1 and C2 produce less vigorous sea breezes as observations indicated (Frank *et al.*, 1967). One of the reasons could be that the convergence zone is advected faster during stronger ambient wind conditions. However, the convergence zone remains nearly stationary under light ambient winds and thus has more time to develop in its original environments. These results show that the magnitude of the ambient wind is also an important factor in the formation of sea breeze convergence zones and the associated convection.

5. Conclusions

The relationship between sea breeze and convection was investigated over the Florida peninsula for typical summer days by using a higher order turbulence closure mesoscale boundary-layer model. The numerical sensitivity experiments reported in this study were based on the observational fact that an important factor controlling convective activities over the Florida peninsula is the formation of the sea breezes. Therefore, the influence of the two dominant wind directions was examined. In addition, the influence of the magnitude of the ambient wind, surface roughness and lake Okeechobee were also investigated.

It was concluded that spatial and temporal variations of the sea breeze convergence zones and hence convective activities are controlled by the characteristics of the ambient flow. Under a southeasterly ambient wind, a secondary convergence zone forms first along the east coast and moves inland with a speed dependent on the magnitude of the ambient wind, while a primary convergence zone develops along the west coast and remains almost stationary during the day. Under a southwesterly ambient wind, the secondary convergence zone forms along the west coast and moves inland, while a stationary primary convergence zone occurs along the east coast. Most of the intense convection and large rainfall occur for both the southeasterly and the southwesterly cases in the primary sea breeze convergence zone, while somewhat weaker cumulus clouds and very little rainfall occur in the secondary sea breeze convergence zone. This indicates that an impor-

tant factor controlling convective activities over the Florida peninsula is the formation of sea breezes. However, the location and intensity of the convection are also controlled by local terrain inhomogeneities (such as coastal irregularities). In contrast to the southeasterly and southwesterly ambient wind cases, under light ambient winds, the predicted features are almost equally prevalent on both the west and the east coasts of the peninsula and show little movement during the day. Maximum vertical motions and associated rainfall occur in regions where the curvature of the coastline is greatest and where sharp turns of the flow occur. Southeasterly ambient winds produce more intense convection as compared to southwesterly ambient winds because of the coastal irregularities along the west coast. Maximum magnitudes in both cases were smaller than those predicted under light ambient winds.

Experiments conducted to examine the effect of lake Okeechobee have shown that the lake has its own mesoscale circulation because of its large size. The resultant divergent flow due to differential heating between the lake and the land causes a persistent cloudless region over the lake during the day in all cases. This cloud-free region is well observed by satellite pictures. The results also indicate that temporal and spatial variations of convection in south Florida are highly correlated with the presence of the lake. Finally, increased land surface roughness appears to influence the location and magnitude of the convective activities by increasing the intensity of the vertical turbulent transport of heat and momentum.

Acknowledgements

The authors wish to thank Dr. Ching-Yuang Huang for several helpful suggestions. We would like also to thank the North Carolina Super Computer Center (NCSC) for the use of computer facilities. This work was supported by the Atmospheric Sciences Division, National Science Foundation under Grant ATM-88-01650.

References

Businger, J. A., Wyngaard, J. C., Izumi, Y. and Bradley, E. F.: 1971, 'Flux-Profile Relationships in the Atmospheric Surface Layer', *J. Atmos. Sci.* **28**, 181–189.

Byers, H. R. and Rodebush, H. R.: 1948, 'Causes of Thunderstorms of the Florida Peninsula', *J. Meteorol.* **5**, 275–280.

Cotton, W. R.: 1975, 'On Parameterization of Turbulent Transport in Cumulus Clouds', *J. Atmos. Sci.* **32**, 548–564.

Cotton, W. R., Pielke, R. A. and Gannon, P. T.: 1976, 'Numerical Experiments on the Influence of the Mesoscale Circulation on the Cumulus Scale', *J. Atmos. Sci.* **33**, 252–261.

Estoque, M. A.: 1962, 'The Sea Breeze as a Function of Prevailing Synoptic Situation', *J. Atmos. Sci.* **19**, 244–250.

Fisher, E. L.: 1961, 'A Theoretical Study of the Sea Breeze', *J. Meteorol.* **18**, 215–233.

Foote, G. B.: 1991, 'Scientific Overview and Operations Plan: Convection and Precipitation/Electrification Experiment (CaPE)', NCAR Technical Report, Boulder, Colorado, 145pp.

Frank, N. L., Moore, P. L. and Fisher, G. E.: 1967, 'Summer Shower Distribution over the Florida Peninsula as Deduced from Digitized Radar Data', *J. Appl. Meteorol.* **6**, 309–316.

Huang, C. Y.: 1990, 'A Mesoscale Planetary Boundary Layer Model for Simulations of Topographically Induced Circulations', Ph.D Dissertation, North Carolina State University, 253 pp.

Huang, C. Y. and Raman, S.: 1991, 'A Comparative Study of Advection Schemes with a Modified WKL Scheme', *Mon. Wea. Rev.* **119**, 2900–2918.

Huang, C. Y. and Raman, S.: 1991a, 'Numerical Simulation of January 28 Cold Air Outbreak During "GALE" I, The model and Sensitivity Tests of Turbulence Closures', *Boundary-Layer Meteorol.* **55**, 381–407.

Huang, C. Y. and Raman, S.: 1991b, 'Numerical Simulation of January 28 Cold Air Outbreak During "GALE" II, The Mesoscale Circulation and Marine Boundary Layer', *Boundary-Layer Meteorol.* **56**, 51–81.

Klemp, J. B. and Durran, D. R.: 1983, 'An Upper Boundary Condition Permeating Internal Gravity Wave Radiation in Numerical Mesoscale Model', *Mon. Wea. Rev.* **111**, 430–444.

Mahrer, Y. and Pielke, R. A.: 1977, 'The Effects of Topography on the Sea and Land Breezes in a Two-Dimensional Numerical Model', *Mon. Wea. Rev.* **105**, 1151–1162.

McPherson, R. D.: 1970, 'A Numerical Study of the Effect of a Coastal Irregularity on Sea Breeze', *J. Appl. Meteorol.* **9**, 767–777.

Mellor, G. L. and Yamada, T.: 1982, 'Development of a Turbulence Closure Model for Geophysical Fluid Problems', *Rev. Geophys. Space Phys.* **20**, 851–875.

Miller, M. J. and Thorpe, A. J.: 1981, 'Radiation Conditions for the Lateral Boundaries of Limited Area Numerical Models', *Q. J. R. Meteorol. Soc.* **107**, 615–628.

Neumann, C. J.: 1971, 'The Thunderstorm Forecasting System at the Kennedy Space Center', *J. Appl. Meteorol.* **10**, 921–936.

Neumann, J. and Mahrer, Y.: 1971, 'A Theoretical Study of the Land and Sea Breeze Circulations', *J. Atmos. Sci.* **28**, 532–542.

Orlanski, I.: 1976, 'A Simple Boundary Condition for Unbounded Hyperbolic Flows', *J. Comput. Phys.* **21**, 251–269.

Pearson, R. A.: 1973, 'Properties of the Sea Breeze Front as Shown by a Numerical Model', *J. Atmos. Sci.* **30**, 1050–1060.

Pielke, R. A.: 1974, 'A Three-Dimensional Model of the Sea Breezes over South Florida', *Mon. Wea. Rev.* **102**, 115–139.

Pielke, R. A. and Cotton, W. R.: 1977, 'A Mesoscale Analysis over South Florida for a High Rainfall Event', *Mon. Wea. Rev.* **105**, 343–362.

Pielke, R. A. and Mahrer, Y.: 1978, 'Verification Analysis of the University of Virginia Three-Dimensional Mesoscale Model Prediction over South Florida for July 1, 1973', *Mon. Wea. Rev.* **106**, 1568–1589.

Warming, R. F., Kutler, P. and Lomax, H.: 1973, 'Second-and Third-Order Noncentered Difference Schemes for Nonlinear Hyperbolic Equations', *AIAA J.* **11**, 189–196.